Carbon nanofibers (CNFs) dispersed in ultra-high performance concrete (UHPC): mechanical property, workability and permeability investigation

Linfei Li[a,b,*], Boning Wang[b], Mija H. Hubler[a,b]

[a] University of Colorado, Department of Civil and Environmental Engineering, Boulder, CO 80309, USA
[b] University of Colorado, Materials Science & Engineering Program, Boulder, CO 80309, USA
[*] Corresponding author.
E-mail address: linfei.li@colorado.edu (Li, L.)

Abstract: This paper presents experimental data on the effect of carbon nano-fiber (CNF) dispersion on mechanical behavior, workability, and permeability of ultra-high-performance concrete containing CNF (UHPC-CNF). The addition of CNFs in concrete has been shown to provide improved performance. However, an inhomogeneous distribution of CNFs in the cement matrix can result in no impact or decreased mechanical performance. Due to the van der Waal's forces and hydrophobic surface properties of the CNFs, good dispersion in mix fluids and cement paste is challenging. Experimental studies of UHPC-CNF with different dispersion methods are provided. Further mixing with optimized UHPC paste allowed for the investigation of the optimal dosage of CNFs, impact on porosity, compressive strength, flexural strength, hydration rate, and slump. Scanning electron microscopy (SEM) analysis visually revealed the effect of dispersion. The results indicate that shear mixing and subsequent ultrasonic dispersion with chemical surfactants can provide a well-dispersion liquid admixture of CNFs resulting in high mechanical performance of UHPC-CNFs composites. The water permeability and chloride resistance of optimized UHPC-CNFs composites were further evaluated with the wicking test and ponding test to reveal improved performance for these properties as well.

Keywords: carbon nanofibers (CNFs), dispersion, durability, scanning electron microscope (SEM), ultra-high performance concrete (UHPC)

1 Introduction

Previous research on cementitious materials has sought a new cement-based construction material which can break through the performance delivered by regular concrete [1-4]. Among these developments, ultra-high performance concrete (UHPC), developed in 1994, successfully became one of the most practical cementitious materials applied on the construction site [5-7]. Compared to regular concrete, UHPC can provide extraordinarily high compressive strength up to 300 MPa with reasonable flexural strength (20 MPa without fibers and over 40 MPa with metal, synthetic or organic fibers) [8-11]. The key to UHPC is to lower the water-to-cement ratio, which can effectively increase the packing density of the hardened material and further improve the performance [12, 13]. The incorporation of silica fume adds a pozzolanic reaction between cement and silica fume which helps the transition from portlandite to calcium silica hydrate (C-S-H). With more C-S-H, improved mechanical strength can be achieved [14].

Although UHPC can provide outstanding compressive strength and stiffness, the low tensile strength and flexure toughness cannot be changed based on the chemistry of the material. Ultra-high performance fiber reinforced concrete (UHPFRC) is the solution for controlling crack propagation [15]. The bonded macro-fibers can compensate for the low tensile/flexure strength of the cementitious material. Different types of macro-fibers have been applied in cementitious materials, such as steel fibers, polypropylene fibers, and glass fibers [16]. These fibers can effectively mitigate crack propagation of the cementitious material and dissipate fracture energy [17]. However, from a micromechanics point of view, the crack widths in cementitious materials start at the nanometer scale [18]. Traditional reinforcing fibers have diameters at the micrometers scale so they cannot control nanoscale crack propagation nor prevent the nucleation of cracks at the nanoscale [19]. Therefore, the addition of nanoscale fibers into the cementitious material has become a recent topic of interest [20, 21]. Nanoscale fibers in cementitious materials not only act through a bridging effect after cracks appear, but also provide an elongated shape that can cause the cracks to travel further around these stiff inclusions. Previous publications [22-25] show that the bridging effect happens on cementitious materials with the dosage of nanoscale fibers as low as less than 0.1 cwt% and as high as 2 cwt%. Among all available nanofibers, carbon nanofibers (CNFs) are the most commonly used in research because of their excellent mechanical properties which include a tensile strength of 2-5 GPa and an elastic modulus of 300 GPa [21, 26]. Well dispersed CNFs can effectively improve not only the concrete tensile strength, but also the compressive strength and electrical conductivity for strain monitoring, and damage evaluation [27].

Due to the van der Waal's forces and the hydrophobic property of the fibers, CNFs tend to bundle together during the mixing stage with cementitious material [28, 29]. An inhomogeneous distribution of CNFs in concrete can result in no impact or decreased mechanical performance. In addition, the atomically smooth surface of bundled CNFs also causes an unstable interfacial bond strength with the cement matrix [30]. Many studies have focused on addressing these dispersion challenges in the past few decades and they can be separated into four main approaches: premixing, fiber surface pre-treatment, ultrasonic dispersion, and chemical bonding [25-41]. Chung used different types of admixtures to pre-mix with CNFs, such as silica fume, polymer solution, polymer particles, silane, etc. [31]. Chang used the same premix method but choose sodium dodecyl sulfate as the admixture [32]. The selection of the pre-mix should consider both the physical effect (friction generated from fine particles) and chemical effect (surface property changes due to the added chemicals). The second method introduced is to pre-treat the surface of the fiber, such as by ozone treatment, silane coating, and acid treatment [25, 29, 31, 33]. The objective of these pre-treatments is to change the surface property of CNFs from hydrophobic to hydrophilic. Compared with acid treatment, adding chemical surfactant saves time and does not damage the fibers. In the following years, ultrasonic dispersion technology was introduced as a CNFs dispersion method [34-37]. Rather than adding chemical surfactants or pre-treatment of the fiber, the ultrasonic wave can help break the van der Waal's forces between fibers [29]. The fibers are uniformly distributed in the base liquid after ultrasonic dispersion. However, after mixing with cementitious material, SEM images of the hardened cement showed that CNFs re-agglomerate together [34]. This is because the hydrophobic surface property of the CNFs is not changed in the ultrasonic dispersion process. Therefore, a combined dispersion technique which breaks van der Waal's forces and affects the surface properties may be best. With proper dispersion improved mechanical properties and electric conductivity have been achieved on cementitious materials by researchers [34-37]. In recent years, interdisciplinary research has been conducted between civil engineering and chemical engineering to provide ways to chemically bond CNFs onto the raw materials used in cement. This is called cement hybrid material (CHM) [38-41]. The production process of CHM can be cheap and the feedback from both mechanical and electric properties from hardened cementitious material are convincing. A full understanding of dispersion techniques will be needed to address the needs of these new composite fibers.

Although there have been many successful stories of improving the mechanical behavior of cementitious material with the addition of carbon nanomaterials (CNFs, carbon nanotubes, and carbon nanoplatelets), few studies can be found that combine carbon nanomaterials with UHPC [42-44]. This is because the surface area of carbon nanomaterials is large, which can increase the amount of liquid required for carbon nanomaterial dispersion. Therefore, most traditional dispersion techniques are not conductive for UHPC due to its extremely low water-to-cement ratio. Furthermore, even if well-dispersed CNFs in liquid form are available, adding the large surface area of CNFs into cement slurry can cause a decrease in workability. Thus, the compaction of UHPC can be affected and a homogenous mix will be hard to achieve. The workability increase can be solved by adding more water or more high range water reducer (HRWR), which increases the air voids in the hardened cement and consequently decreases the mechanical performance and durability of the cementitious material. In previous studies, most researchers begin by adding CNFs from 0.1% weight of cement up to 1% weight of cement [33, 38]. Only a few researchers have studied the addition of CNFs over 1% weight of cement [39]. The percolation threshold of CNFs which will improve the mechanical behavior and durability of UHPC stands to be determined.

Therefore, a comprehensive study of UHPC-CNF composites is conducted in this paper which optimizes the UHPC mix design and selects the most effective dispersion technique based on the corresponding improvement of mechanical, workability, and permeability performance. Fig.1 provides a flow chart of the research approach in this study and the tests conducted for each module. UHPC mix designs were developed based on those published in literature and industry reports. One of these mix designs was selected as the 'optimal mix design' based on targeted performance metrics, i.e., compressive strength and slump. The optimal mix design was then applied as the base UHPC mixture. Different CNF dispersion techniques and sensitivity analyses were reported considering the optimal dispersion time, dispersion method, and amount of HRWR applied, etc. The flexural properties of UHPC-CNF composites, porosity measurement, and SEM images were used to evaluate the effectiveness of the dispersion of the CNFs. Then, the selected UHPC-CNF composite behavior was assessed mechanically by compression testing, in terms of workability by slump test and temperature evolution measurement, and permeability by wicking and ponding tests.

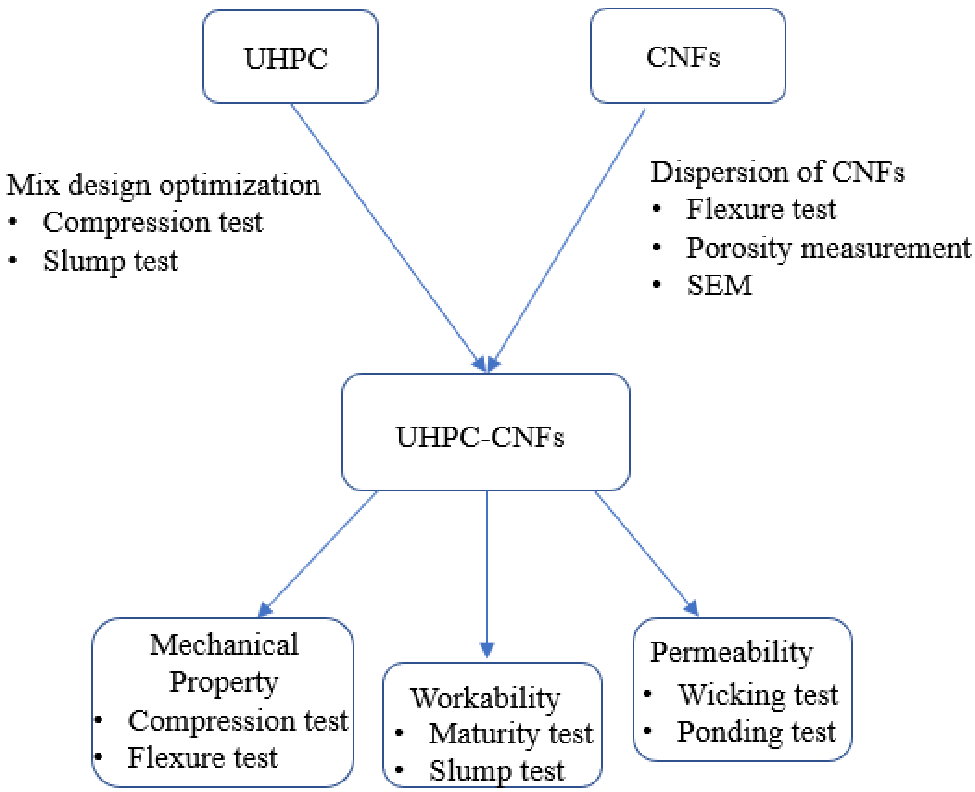

Figure 1 Research guideline and test conducted

2 Materials and Sample Preparation

2.1 Materials

Type I Portland cement and silica fume were utilized as the binding material. Table 1 lists the chemical composition of cementitious material. The size of the fine aggregate in the mix design is specified to be smaller than 5 mm following ASTM C1856 [45]. Thus, the all-purpose natural sand, Milliken USGA natural sand, and silica powder were selected for making UHPC. The grading of all-purpose sand followed ASTM C33 [46]. The particle size distributions (PSDs) of the all-purpose sand and Milliken USGA sand are shown in Fig. 2. The CNFs were manufactured through chemical vapor deposition (CVD). The dimensions and properties of CNFs are provided in Table 2. In addition, a polycarboxylate-based HRWR was used to improve the dispersion of the CNFs and the workability of the UHPC slurry. Methylcellulose and polyacrylic acid were introduced as the chemical surfactants to adjust the CNF surface property.

Table 1 Chemical composition of cementitious material

Chemical composition (wt%)	Cement	Silica fume
SiO_2	20.2	98.4
Al_2O_3	4.2	0.2
Fe_2O_3	3	0.01
MgO	1.2	0.1
CaO	65	0.2
Na_2O	0.5	0.15

K_2O	0.3	0.2
P_2O_5	-	0.03
SO_3	3.5	0.1
Insoluble residue	0.25	-
Loss on ignition	2.7	0.5

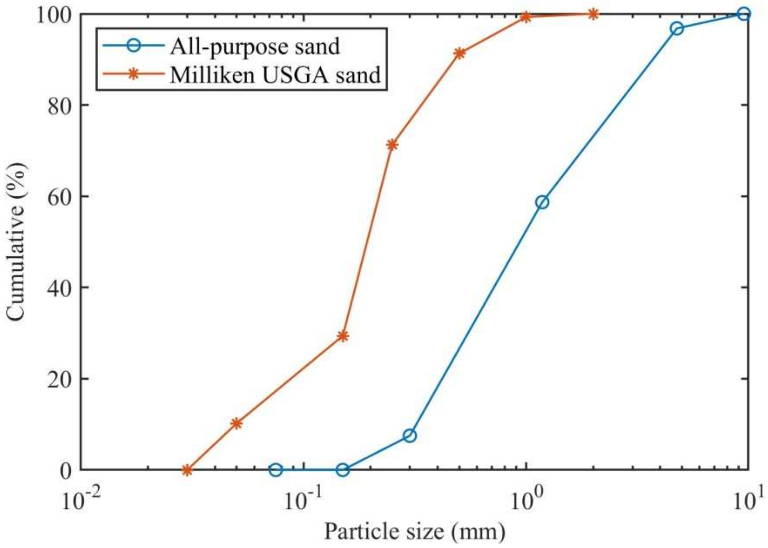

Figure 2 PSDs of all-purpose sand and Milliken USGA sand

Table 2 Dimensions and properties of CNFs

Dimensions and Properties	
Length (um)	50-200
Diameter (nm)	100-200
Density (g/cm^3)	1.55-1.70
Purity (wt%)	>98
Surface area (m^2/g)	20-30
Elastic modulus (GPa)	240
Tensile strength (GPa)	4.75

2.2 Sample preparation

2.2.1 Mixing procedure

A lab-scale bowl mixer with multi-speed control was adopted to mix the slurry. For mixing the UHPC, the dry constituents were premixed for 2 mins at 60 rpm to achieve a homogenous dry mix. Half of the HRWR and water were premixed and then added into the mixer mixing at 120 rpm. After another 2 mins, the remaining HRWR was added. Over 10 mins of mixing were applied until a homogenous slurry was obtained. To mix the UHPC-CNF, the CNFs were premixed with water and chemical surfactants (methylcellulose/polyacrylic acid/part of HRWR) to build a liquid admixture. This liquid admixture was first added to the homogenous dry mix and mixed using the methods for UHPC [8]. After 2 mins, the remaining HRWR was added. It was noticed that the dry materials cannot bind together until the HRWR started to act. This process could take up to 20 mins.

2.2.2 Sample prepared for compression test

Three curing methods for the sample were prepared for each mix design (with and without CNFs) [47-50]. Each group had three repeated cylinder samples with diameter of 5.08 cm and height of 10.16 cm. For group 1, the samples were submerged in limewater at 90 °C for 7 days. Samples were demolded after the first 24 hours [50]. The lime saturated curing environment can reduce the leaching of portlandite (CH) [51]. Previous research stated that CH is relatively mobile in the cement paste matrix and can easily be leached out. Dissolution and leaching of CH increases the porosity within the cement system and decreases the pH level which consequently compromises strength and durability of cement-based products [52, 53]. For group 2, the samples were cured at laboratory temperature of 23 °C with relative humidity of 75% for 7 days [50]. The remaining samples from group 3 were cured at the laboratory temperature of 23 °C with relative humidity of 75% for 28 days. After demolding, the top and bottom surfaces of the cylinder were polished. The objective of this process is to avoid any stress concentration during the compression test, which could break the sample before the real peak load is achieved. Note that the sulfur capping was not applied for UHPC material due to its low strength.

2.2.3 Sample prepared for flexure test

Following ASTM C348 [54], 40 × 40 × 160 mm prism samples were prepared. In total, over 40 groups of samples were prepared. Three repeated prisms were cast for each group. The prisms were cured one day in the molds and then were demolded and transferred into limewater at the laboratory temperature of 23°C for 7/28 days [50]. Three repeated prisms were cast for each group.

2.2.4 Sample prepared for temperature evolution measurement

Three cylinder samples were prepared for the temperature evolution measurement [55]. One of the samples was cast without CNFs and the other two were cast with CNFs with different dispersion methods. To accommodate the embedded temperature sensors [56], the 10.16 cm diameter of the cylinder samples prepared for the temperature evolution measurement is larger than the one prepared for compression test. The height of the sample is 10.16 cm.

2.2.5 Sample prepared for wicking test

Three groups of 5.08 × 10.16 cm cylinder samples were prepared, and three repeated samples were cast for each group following ASTM C1585 [57]. All cylinder samples were cured at the laboratory temperature of 23 °C with relative humidity of 75% for 28 days. To be consistent with the compression test, the same curing method was used. The samples were demolded before the test.

2.2.6 Sample prepared for ponding test

Three groups of samples were prepared with two repeated samples for each group according to ASTM C1543 [58-60]. To collect chloride profiles at different depths and different time, large size samples were required and cast with a diameter of 7.62 cm and height of 15.24 cm. The same curing procedure was followed as in the wicking test procedure. After 28 days, samples were demolded and ready for testing.

3 Experimental procedure

3.1 UHPC mix design optimization

From the ASTM standard C1856, the minimum requirement of compressive strength of UHPC is 120 MPa at 28 days of curing [45]. Table 3 presents five different mix designs of UHPC without CNFs. The optimal mix design was selected based on the test results collected from the compression test and slump test for each group, which followed ASTM C39 and ASTM C143 [61, 62].

Table 3 UHPC mix designs (wt%)

Specimen	w/c	Cement	Water	All-purpose sand	Milliken USGA sand	SF	HRWR	Silica powder
1	0.22	31.62	6.97	-	44.28	7.89	1.33	7.89
2	0.23	30.05	6.91	-	51.92	9.75	1.37	-
3	0.22	38.68	8.53	-	32.54	9.66	0.94	9.66
4	0.21	34.45	7.43	-	34.93	6.90	1.30	14.99
5	0.18	35.84	6.45	49.52	-	6.63	1.55	-

Notes: ‘w/c’ is the water-to-cement ratio.

3.2 Dispersion of CNFs

3.2.1 Different dispersion techniques

To effectively disperse the bundles of CNFs caused by hydrophobic surface property and Van der Waal’s forces, different combinations of dispersion methods and chemical surfactants were investigated. The combinations are summarized in Table 4 with detailed information provided. It is noticed that all these dispersion methods were referred and modified from the published proven methods [30, 31, 34-37]. For comparison, the ‘Control’ sample (D0) and the UHPC-CNFs sample without any treatment (D1) were prepared first. Different dispersion methods were considered with bowl premixing only (D3, D4), magnetic stirrer premixing only (D5, D6), ultrasonic dispersion only (D7, D8, D9), and the combination of magnetic stirrer premixing and ultrasonic dispersion (D10, D11). In addition, to test the effectiveness of changing the surface property of CNFs, different types of chemical surfactants were selected and combined with the dispersion methods provided above: Methylcellulose (D2, D4, D6, D9, D11), Polyacrylic acid (D8), HRWR (D3, D5, D7, D10).

Note that when applying the HRWR as a chemical surfactant for CNFs dispersion, the HRWR used for mixing was separated in two parts: one part was used for dispersion of the CNFs in liquid, and another was directly added into the dry ingredients. The total amount of HRWR was kept as a constant. The porosity measurement (ASTM C830) [63], flexure test, and the image analysis (SEM) were then applied on samples with 7-days curing to evaluate the effectiveness of CNF dispersion in terms of performance and visual inspection.

Table 4 Different dispersion techniques

Specimen	Description
D0 (Control)	Adopted optimized UHPC mix design without CNFs as the control sample.
D1	Considered CNFs as dry ingredients without any treatment.
D2	Same as D1 but with 0.1 cwt% of Methylcellulose added.

D3	Premixed CNFs with water and part of HRWR by using bowl premixing for 10 mins.
D4	Same as D3 but with 0.1 cwt% of Methylcellulose added during premixing.
D5	Premixed CNFs with water and part of HRWR by using magnetic stirrer premixing for 10 mins.
D6	Same as D5 but with 0.1 cwt% of Methylcellulose add during premixing.
D7	Applied ultrasonic dispersion on CNFs with water and part of HRWR for 10 mins.
D8	Same as D7 but with 0.01 cwt% of Polyacrylic acid during ultrasonic dispersion.
D9	Same as D7 but with 0.1 cwt% of Methylcellulose during ultrasonic dispersion.
D10	Conduct D5 first, then transferred the liquid to run D7.
D11	Same as D10 but with 0.1 cwt% of Methylcellulose added during the whole process.

Notes: 'cwt%' is the weight percentage of cement; 'part of HRWR' means the HRWR:CNFs=5:1; The proportion between HRWR and CNFs is based on mass; The amounts of CNFs used was kept as 0.1 cwt% for each group; The bowl premixing was done at 140 rpm; The magnetic stirrer premixing was done at 1200 rpm. The ultrasonic dispersion time was 10 mins.

3.2.2 Sensitivity analysis

To further optimize the dispersion process, a sensitivity analysis was conducted on samples after the most effective dispersion technique was found, such as adjusting the ultrasonic dispersion energy, adjusting the amount and proportion of HRWR used, optimizing the amounts of CNFs added, and considering the effect of different types of fine aggregate. The different modules of sensitivity analysis are provided in Table 5 to Table 9. The ultrasonic dispersion process was conducted by using a 20kHz Ultrasonic Processor (Ultrasonics Inc.) with an output power of 450 W.

Table 5 Different ultrasonic dispersion energies delivered

Specimen	Description	UE_I
T1	2 min dispersion time	2
T2	4 min dispersion time	4
T3	6 min dispersion time	6
T4	10 min dispersion time	10

Notes: The most effective dispersion technique was adopted with 0.1 cwt% of CNFs for all groups (HRWR:CNFs=5:1); Three identical specimens were prepared for each group.

The ultrasonic energy indicator is related to the dispersion time and ultrasonic amplitude (equation 1) [64]. In this context, the ultrasonic dispersion energy is controlled by dispersion time and the ultrasonic amplitude was kept as constant of 100%, shown in Table 5.

$$UE_I = \left(\frac{UE_T}{UE_m}\right)^{UA} = (t_s)^{UA} \quad (1)$$

where UE_I is the ultrasonic energy indicator; UE_T is the total ultrasonic energy (J/ml); UE_m is the ultrasonic energy delivered to the solution in a minute (J/ml/mins); UA is the ultrasonic amplitude from 0% to 100%; t_s is the dispersion time in minute (mins).

It is noted that the 100% amplitude is applied for all the dispersion in this manuscript to simplify the calculation of ultrasonic energy indicator. The calculated UE_I is shown in Table 5.

Table 6 Different amounts and proportions of HRWR involved

Specimen	Description
H0 (control)	Adopted optimized UHPC mix design without CNFs as the control sample.
H1	HRWR:CNFs=5:1 applied for ultrasonic dispersion.
H2	HRWR:CNFs=10:1 applied for ultrasonic dispersion.
H3	HRWR:CNFs=5:1, and 0.1 cwt% of Methylcellulose applied for ultrasonic dispersion.
H4	HRWR:CNFs=10:1, and 0.1 cwt% of Methylcellulose applied for ultrasonic dispersion.
H5	Same as H1, but the HRWR used for ultrasonic dispersion was counted as extra for mixing.
H6	Same as H2, but the HRWR used for ultrasonic dispersion was counted as extra for mixing.
H7	Same as H3, but the HRWR used for ultrasonic dispersion was counted as extra for mixing.
H8	Same as H4, but the HRWR used for ultrasonic dispersion was counted as extra for mixing.

Notes: The most effective dispersion technique was applied with 0.1 cwt% of CNFs for all groups; The ultrasonic dispersion time is 10 mins; Three identical specimens were prepared for each group.

The HRWR used in concrete mixing can effectively help to decrease the use of water, which further provides the high strength of cementitious material. Both the Methylcellulose and the HRWR are surface surfactants that can change the surface properties of CNFs. Therefore, an optimized amount and proportion of HRWR used for CNFs dispersion and the combination of HRWR with Methylcellulose were analyzed from H1-H4 in Table 6. In addition to changing the CNFs and HRWR proportions of 1:5 and 1:10 in dispersion, considering the part of the HRWR used for CNF dispersion as extra rather than splitting from the original total amount, shown in H5-H8 in Table 6, was considered.

Table 7 Different amounts of CNFs involved

Specimen	Description
0.05%CNFs	Mixed UHPC with 0.05 cwt% of CNFs
0.10%CNFs	Mixed UHPC with 0.10 cwt% of CNFs
0.20%CNFs	Mixed UHPC with 0.20 cwt% of CNFs
0.50%CNFs	Mixed UHPC with 0.50 cwt% of CNFs

Notes: The most effective dispersion technique and chemical surfactant were applied (HRWR:CNFs=5:1); The ultrasonic dispersion time is 10 mins; Three identical specimens were prepared for each group.

Four dosages of CNFs were mixed with the base UHPC mixture (0.05, 0.1, 0.2, 0.5 wt% relative to the cement). Once an optimal dispersion technique was obtained, the optimal CNFs dosage was determined based on the results from flexure test following ASTM C348 [54].

Table 8 Different types of fine aggregate applied

Specimen	Description
F1	Adopted screened sand on #16 sieves, but without CNFs.
F2	Adopted screened sand on #16 sieves, apply ultrasonic dispersion only.
F3	Adopted screened sand on #16 sieves, applied magnetics stirring and ultrasonic dispersion.
F4	Adopted screened sand on #60 sieves, but without CNFs.
F5	Adopted screened sand on #60 sieves, applied ultrasonic dispersion only.
F6	Adopted screened sand on #60 sieves, applied magnetics stirring and ultrasonic dispersion.

Notes: The most effective dispersion technique and chemical surfactant were applied (HRWR:CNFs=5:1); The ultrasonic dispersion time is 10 mins; Three identical specimens were prepared for each group.

In Table 8, different sizes of sand were screened from all-purpose sand. To figure out the fine aggregate impact on the dispersion, the sieve analysis was applied on all-purpose sand. Fine aggregate stayed on #16 and #60 sieves were used to in the UHPC-CNFs mix. As the size of fine aggregate for each group is more uniform compared to the all-purpose sand, the more consistent results are expected from the repeated flexure test.

3.3 Mechanical properties

3.3.1 Compression test

The compressive strength of UHPC-CNF composites was experimentally studied in accordance with ASTM C39 [61]. The Material Testing System 810 (MTS 810) was utilized with a force-controlled setup. The loading rate was set up as 103 N/cm^2/sec, which is faster than the loading rate provided (19-30 N/cm^2/sec) in ASTM C39 [61]. The fast loading rate was applied in most UHPC cases due to its extremely high compressive strength [8, 65-67]. In addition to selecting the optimal UHPC mix design from the five mix designs shown in Table 3, another two groups of specimens were prepared to evaluate the CNF improvement on the mechanical properties of UHPC, which use the two most effective dispersion methods. The samples cast and then kept under different curing conditions for different durations as shown in Table 9.

Table 9 Samples prepared for compression test

Specimen	Description
C1-7/28	Reference: UHPC only; cured for 7/28 days.
C2-7/28	UHPC-CNFs; HRWR:CNFs=5:1 for dispersion; cured for 7/28 days.
C3-7/28	UHPC-CNFs; HRWR:CNFs=10:1 for dispersion; cured for 7/28 days.

3.3.2 Flexure test

The three-point flexure test were conducted on UHPC-CNF composites following the ASTM C348 [54]. The Universal Testing Machine (UTM) was used with a load cell capacity of 50 kN. The loading mode was set up as force control with a loading rate of 2750 N/min. In addition to the flexure tests conducted to evaluate the effectiveness of CNFs dispersion, samples cured for 28 days were tested to obtain the maximum stress and maximum strain. A comparison was made between UHPC-CNF composites and UHPC mixture. The flexure toughness was also reported as in the ASTM standard [54].

3.4 Workability

3.4.1 Slump test

The slump test was performed not only to optimize the UHPC mix design, but also to analyze workability of the UHPC-CNFs. The lab-sized mini-slump cone was applied in this test with a top surface of 50-mm diameter, a bottom surface of 100-mm diameter, and a 150-mm height. Compared to the size of standard slump cone, the mini-slump cone used is with the same proportion (height:bottom diameter:top diameter=3:2:1) but half of the size. The results of the mini-slump cone were transferred to standard slump cone values by a factor of 2 to evaluate the absolute slump and workability [68, 69]. The testing procedure followed ASTM C143 [61]. Once a homogenous slurry was achieved, the slurry was immediately transferred to the slump cone with uniform rodding. Seven groups of samples were tested including five groups of UHPC samples and two groups of UHPC-CNFs samples. The five groups of UHPC samples were tested to select the optimal UHPC mix design. The other two groups of UHPC-CNFs samples combined the selected UHPC mix design with the most two successful dispersion methods of CNFs.

3.4.2 Temperature evolution measurement

The influence of CNFs in UHPC on the temperature evolution was studied following ASTM C1074 [55]. Conducting the temperature evolution measurement is important because of the possibility of workability decrease if the CNFs were to help accelerate the hydration process. With a faster temperature evolution, the UHPC-CNF composites would be more difficult to construct onsite. The temperature evolution measurement applied in this test is Concrete Temperature and Maturity Meters (Command Center Inc.). After casting the samples, a temperature sensor was embedded in the center of each sample. The samples were then immediately transferred to an enclosed space with constant temperature of 23°C and kept in there for 48 hours. In the meantime, the temperature change was recorded by the temperature sensors placed in the maturity meter and the data was reported every minute.

3.5 Permeability

3.5.1 Wicking test

The water permeability of UHPC-CNFs composites was experimentally investigated by wicking tests based on ASTM C1585 [57]. To avoid moisture interaction during the test, the top and side surfaces of cylinder samples were sealed by silicon glue after 28 days of curing. Rubber bands were applied on the side surface close to the bottom to avoid the water intrusion between the glue and sample. A container with a flat surface was prepared with 2.54-cm of water inside. All samples were transferred from the air to the container vertically with the bottom surface of cylinder samples exposed to the water, shown in Fig. 3. The samples were then kept in the water and sustained for 9 days. The mass change of each test specimen was then measured to the nearest 0.01 g at scheduled times.

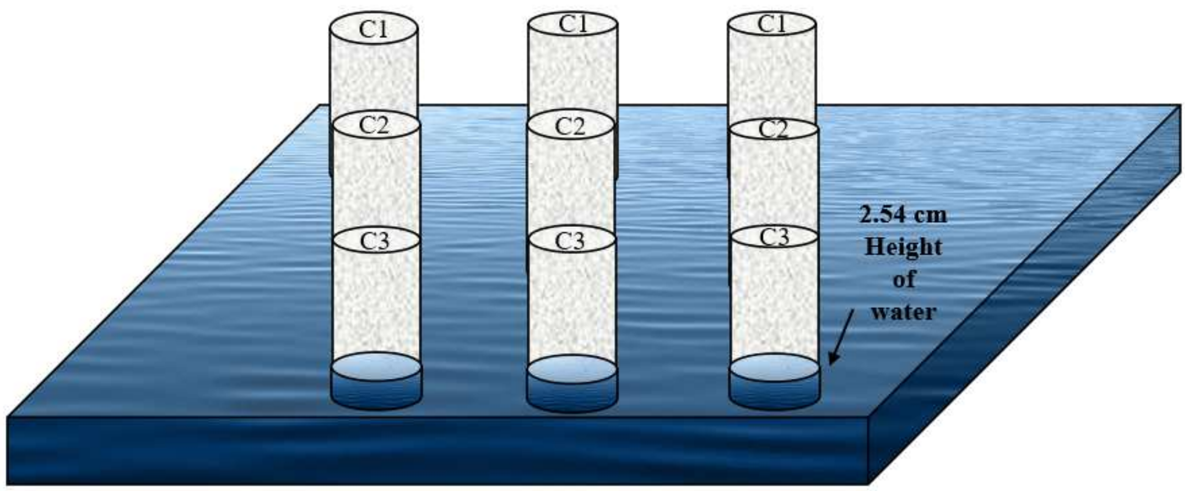

Figure 3 Wicking test setup

3.5.2 Ponding test

The effect of adding CNFs on chloride permeability was investigated with the chloride ponding test, ASTM C1543 [58]. The rapid chloride penetration test (RCPT) in ASTM C1202 was not applied here because of the inappropriate increase of temperature and short-circuit risk caused by the high conductivity of CNFs [9, 70]. Three groups of samples were cast as shown in Table 9. After 28 days of curing, the bottom and side surfaces of cylinder samples were sealed by silicon glue. The plastic circular fence was built on the top of each sample with a tightened stainless steel clamp installed, shown in Fig. 4. A 0.3% of sodium chloride solution was left to pond on the top surface of sample with 3-cm liquid level. The ponding solution was regularly replaced every week to keep a constant concentration of chloride ions. After one-month and three-months of ponding, the pulverized concrete powders from each sample were collected at 12.7-mm depth intervals up to 63.5 mm. Approximately 10 g of collected powders were then transferred into the plastic vials with 50 ml extraction liquid and settled for 24 hours. The extraction liquid is the dilute nitric acid commercially available from Germann Instrument. The calibration liquids were used before measuring the samples for precision. The acid-soluble chloride contents at different depths for each sample were measured by Ion-Selective Electrode (ISE) and compared to each other [59]. It is noted that every measurement was repeated three times and recorded until a stable reading was achieved.

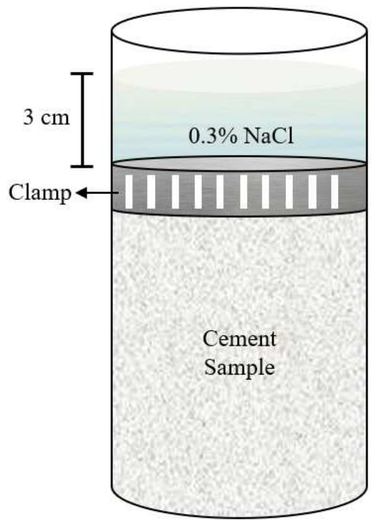

Figure 4 Ponding test setup

4 Results

4.1 UHPC mix design selection

The compressive strengths of UHPC cylinders from five different mix designs under different curing conditions are reported in Fig. 5. Under all curing conditions, mix design 5 provides the highest compressive strengths and with the lowest water-to-cement ratio. Mix designs 2 and 4 show the lowest compressive strengths, below the requirement of UHPC (120 MPa) due to their low water-to-binder ratio. Therefore, mix design 1, 3, and 5 were considered for further testing. Samples cured in hot water at 90 °C can effectively accelerate the hydration process. The improvement of compressive strengths was about 13-17% of compressive strength for samples after 7 days of curing. By 28 days samples exposed to the air for 28 days showed similar compressive strengths compared to the samples cured in the hot water for 7 days. Approximately 12-18% of compressive strengths improvement was found from samples exposed to the air from 7 days to 28 days.

The standard slump test results of UHPC slurry as converted from the mini-slump test are presented in Fig. 6. The highest slump was obtained from mix design 5 with 24.13 cm and the lowest slump was captured from mix design 2 with 16.51 cm. Considering the dense packing of UHPC mixture, the high slump is preferred for practice.

The results obtained from both tests indicated that mix design 5 is the most promising UHPC mixture to be used for the UHPC-CNFs composite. From the slump test results and mix proportions in Table 1, there is no obvious relationship between w/c and slump. In contrast, mix design 5 with the lowest w/c ratio provided the highest slump. This is because of the size of fine aggregate used in mix design 5. The all-purpose sand used in mix design 5 provided a much smaller surface area/weight ratio compared to the USGA sand used in the other four mixes. This means the USGA sand can absorb more water during the mixing stage than all-purpose sand, which resulted in a dry mix. Consequently, due to the low slump of the dry mix, it was hard to deliver a dense packing of the mixture. Furthermore, a relatively small standard deviation was found in compressive strength measures for mix design 5. This may have been since the high slump enabled a homogenous UHPC mixture. There is no evidence showing a change in either compressive strength or slump of UHPC mixture through the addition of silica powder. Therefore, both USGA sand and silica powder were not considered as dry constituents in the selected UHPC mixture.

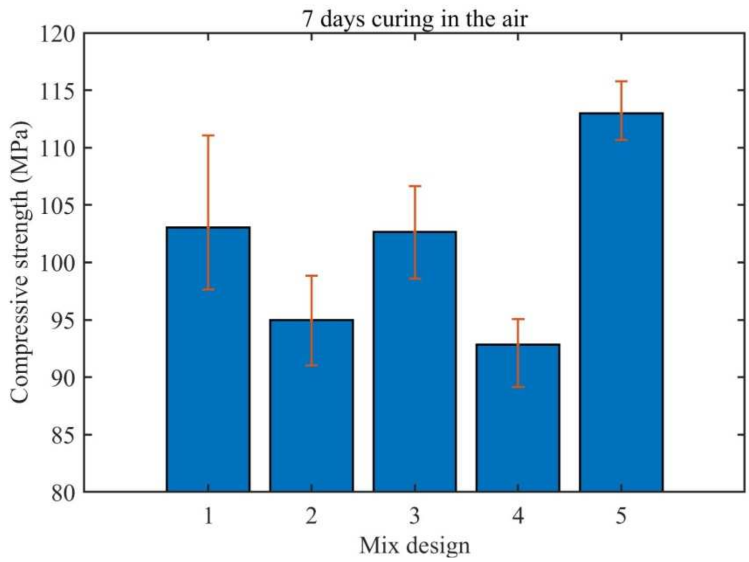

(a)

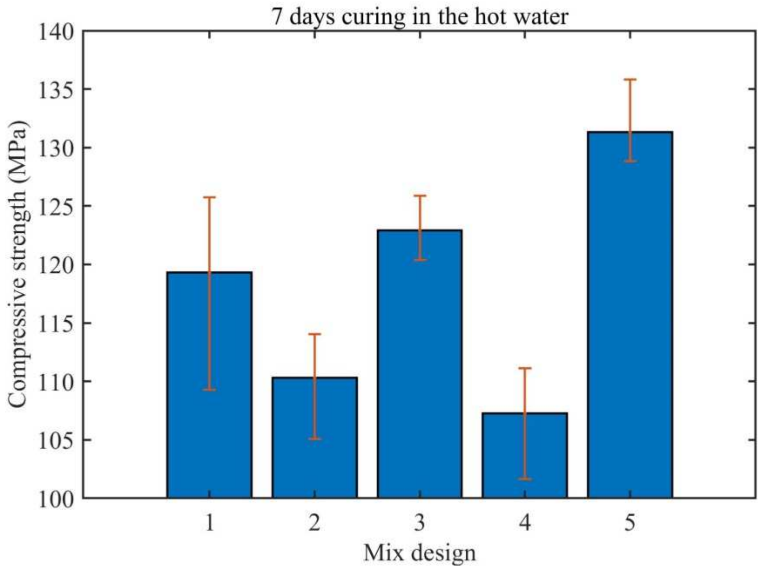

(b)

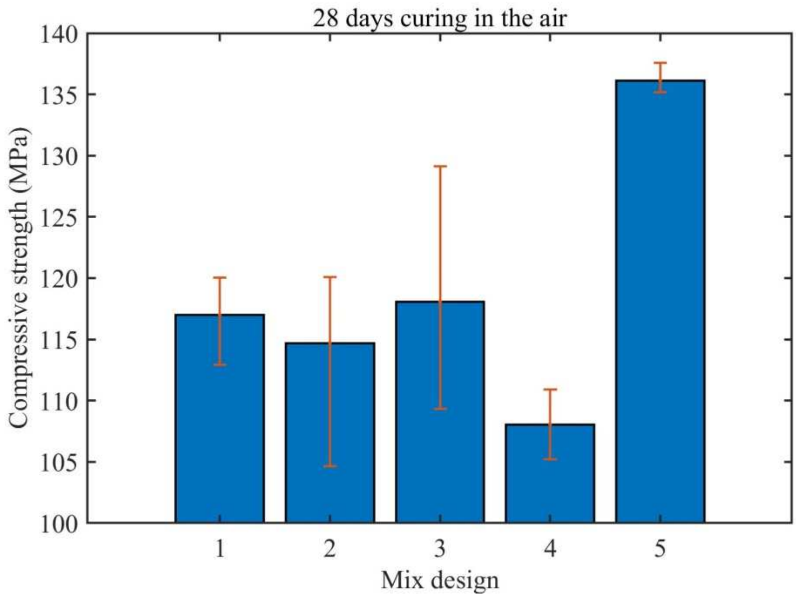

(c)

Notes: The testing results were analyzed from the average value of three identical samples and the error bar provided in the figure offered the minimum and maximum value of the testing results.

Figure 5 Compressive strengths of UHPC mix designs with different curing conditions (a) 7 days of room curing (b) 7 days of hot water curing (c) 28 days of room curing

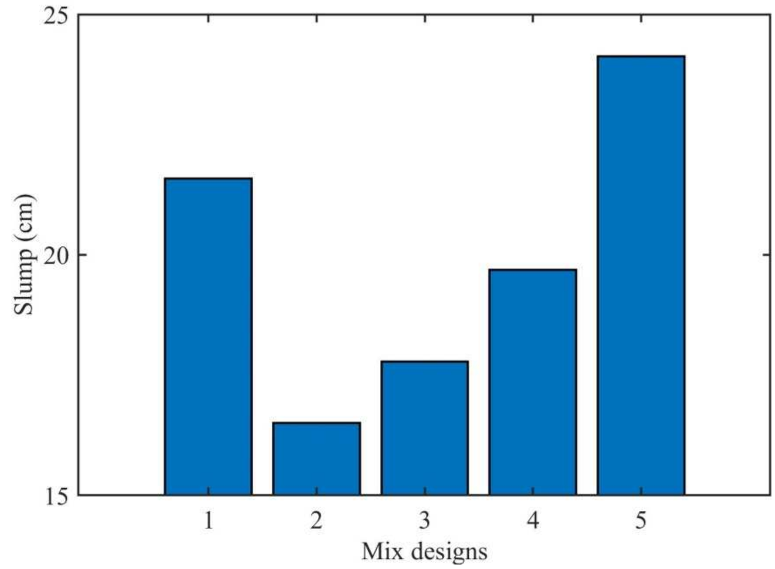

Figure 6 Standard slump of UHPC mix design converted from mini-slump

4.2 Dispersion of CNFs

4.2.1 Different dispersion techniques

The results from porosity measurements and flexure testing are shown in Fig. 7. Starting from the porosity measurements, both treating the CNFs as dry ingredients and premixing the CNFs with low speed caused a poor dispersion of CNFs in UHPC. The inhomogeneous mixing led to an increase of porosity, shown as D1 and D3 in Fig. 7 (a). The addition of methylcellulose was expected to help change the surface property of CNFs from hydrophobic to hydrophilic. However, due to its large surface area, and by keeping the amount of water constant, adding methylcellulose as a chemical surfactant would make the UHPC-CNFs mix became difficult to mix. When setting aside these two factors, an increasing trend of porosities was found, following D2, D4, D6, D9, and D11. In addition to the HRWR and methylcellulose, polyacrylic acid was also applied in D8 as a chemical surfactant. Compared to the porosity measure from D7, a limited effect of improving the packing of UHPC-CNFs is observed through addition of polyacrylic acid. Among all dispersion techniques, D10 provided the lowest porosity of 3.3%. Compared to the UHPC samples with no CNFs (D0), D10 shows over 0.4% porosity decrease. Because D10 dispersed the CNFs better, it can provide a more homogeneous material.

In addition to the porosity measurement, the effect of different dispersion methods on flexural behavior are shown in Fig. 7 (b) and (c). From Fig. 7 (b), dispersion method D3 and D4, using low speed mixing, reported the lowest flexural strain as 0.003236 mm/mm and second lowest flexural strain as 0.003353 mm/mm. All other dispersion techniques provided larger maximum strain compared to the control sample D0. Thus, the functionality of the CNFs in the UHPC mix are reflected in the observed flexural strains to different extents. However, when considering the flexural strength, most of the dispersions showed decreased flexural strength compared to the D0, except for method D10. D10 provided both maximum stress and maximum strain during the flexure test. Compared to the control sample D0, the maximum stress and maximum strain from D10 are improved of 7.3% and 45.53%, respectively. The flexural toughness shown in Fig. 7 (c) is computed from the flexural test data to quantify the capability of the material to resist flexure. It can be calculated by the integral of the area under the load-deflection curve obtained from the flexure test. The results provided in Fig. 7 (c) show that the samples with the D10 dispersion technique provided the largest flexural toughness. The reason could be that D10 dispersed the CNFs the best. The bonding between the CNFs and the ettringite and calcium-silicate-hydrate (CSH) is stronger. Besides, the smaller the porosity is, the denser the material will be. Denser material will have better performance.

Based on the mechanical performance, D10 is selected as the most effective dispersion technique that can deliver a uniform distribution of CNFs in the UHPC matrix. This process can be divided into two steps. In the first step, magnetic stirring was applied at 1200 rpm. In this phase, most of the CNF bundles on the macroscale can be evenly dispersed in the liquid with the help of chemical surfactants. In the second step, the ultrasonic dispersion was employed. In theory, the second step is to avoid the small clusters of bundled CNFs on the microscale held by Van der Waal's forces and further break them into single fibers. Thus, uniform dispersion of CNFs in the liquid can be achieved.

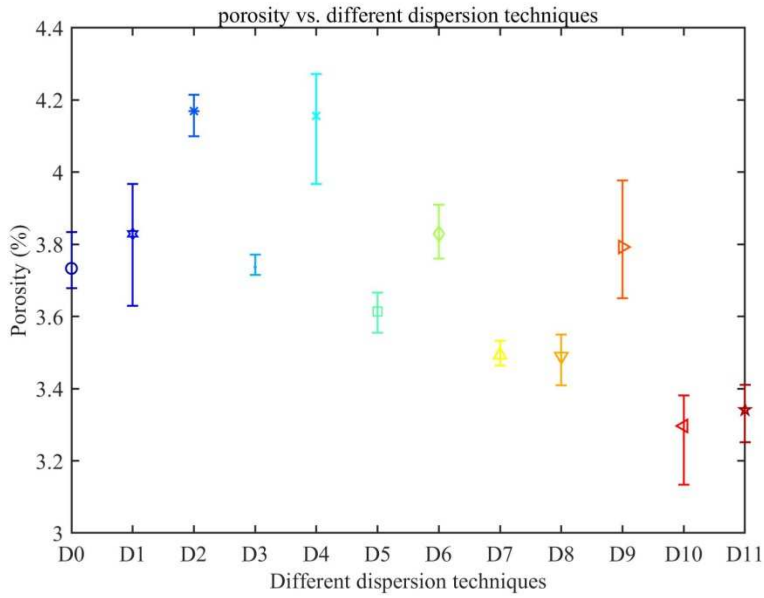

(a)

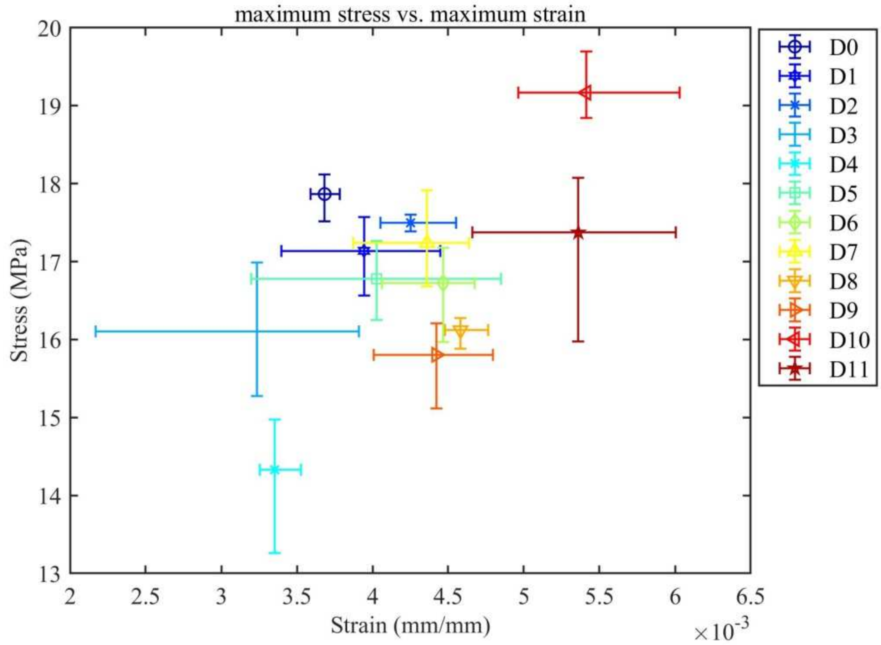

(b)

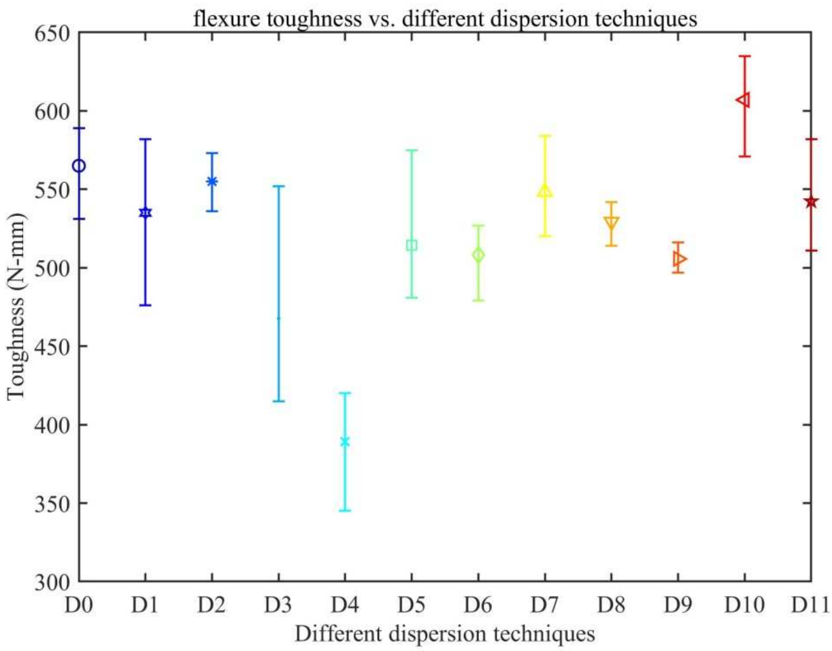

(c)

Notes: The testing results were analyzed from the average value of three identical samples and the error bar provided in the figure offered the minimum and maximum value of the testing results.

Figure 7 UHPC-CNFs from different dispersion techniques (a) porosity measuring (b) maximum stress vs. maximum strain from flexure test (c) flexure toughness

Image-based analysis was used to prove the effectiveness of the developed dispersion technique. For this study, the Hitachi SU 3500 scanning electron microscope (SEM) and the FEI Nova 600 Focused Ion Beam - Field Emission Scanning Electron Microscope (FIB-FESEM) were used with a setting up of 5/10 kV for accelerating voltage and 40 for spot intensity. The SEM was used to target the bundled fiber and the FIB-FESEM was applied to target the well-dispersed CNFs. To further prove the finding from the images and deduce the chemical composition of the objects, the Energy Dispersive X-ray Spectrometer (EDS) analysis was applied. To compare the effectiveness of CNF dispersion in UHPC, samples from D1 and D10 were used for the image and chemical analysis. The samples were cut and cured for two months in the limewater before conducting the image analysis. The imaged surface was further coated with 5.7 nm conductive coating (platinum).

Fig. 8 (a)-(c) shows the SEM image and EDS results of D1. In Fig. 8 (a), the bundled fiber was captured with a substantially large dimension. Two spots were selected for a detailed EDS investigation. Fig. 8 (b) shows the EDS result on spot 1. A large-sized fiber comprised of bundled single CNFs offered high content of carbon (64.4 wt%). On the other side, Fig. 8 (c) focuses on spot 2 without any obvious CNFs. In this case, the calcium, oxygen, and silicon elements provided the most dominant weight proportion. The appearance of the bundled fiber and non-uniformed distribution of CNFs provided evidence that a uniform distribution of CNFs in UHPC was hard to be achieved without the specific dispersion techniques. Fig. 9 (a)-(e) shows the SEM image and EDS results from the D10 sample. The analysis began similarly by targeting the CNFs from the images. From the large-scale observation in Fig. 9 (a), the well-distributed fiber-like products can be found. A further zooming-in process on spot 1 and spot 2 was conducted and images were shown in Fig. 9 (b) and Fig. 9 (c). Fig. 9 (b) shows needle-shaped objectives (Spot 1 in Fig. 9 (a)), and Fig. 9 (c) provides a single CNF appeared (Spot 2 in Fig. 9 (a)). From the EDS results shown in Fig. 9 (d) and (e), it can be seen that spot 3 picked from Fig. 9 (b) was not a CNF but CSH and spot 4 picked from Fig. 9 (c) was a single CNF. In addition, the bundled CNF shown in Fig. 8 (a) cannot be found from the D10 sample but single CNFs, which means a good dispersion of CNFs in UHPC achieved with visual confirmation of the dispersion technique D10.

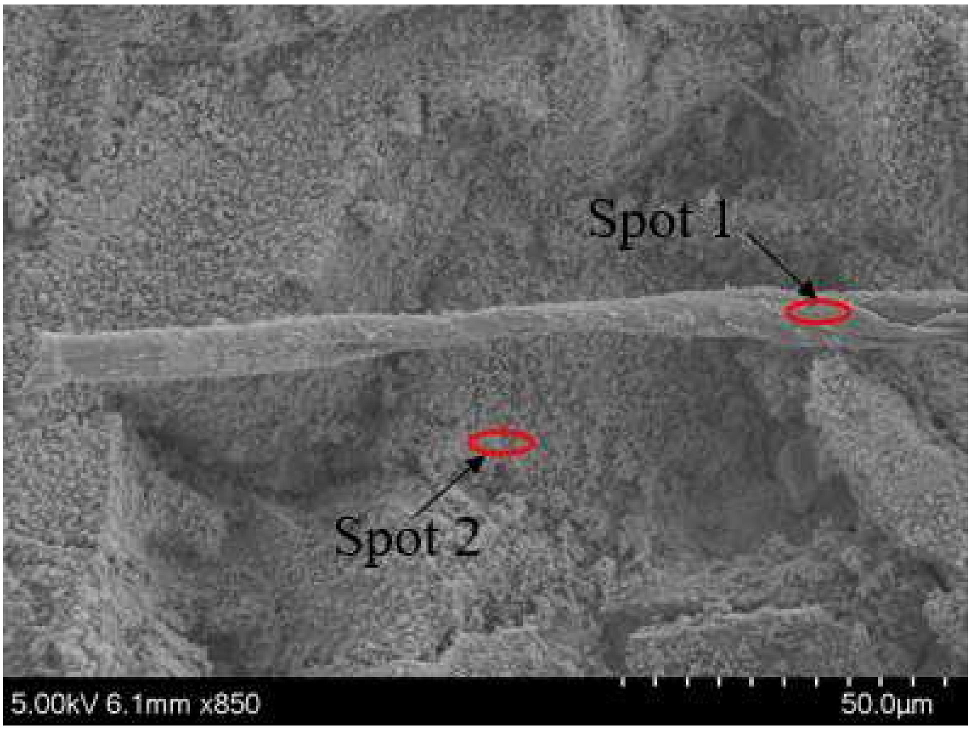

(a)

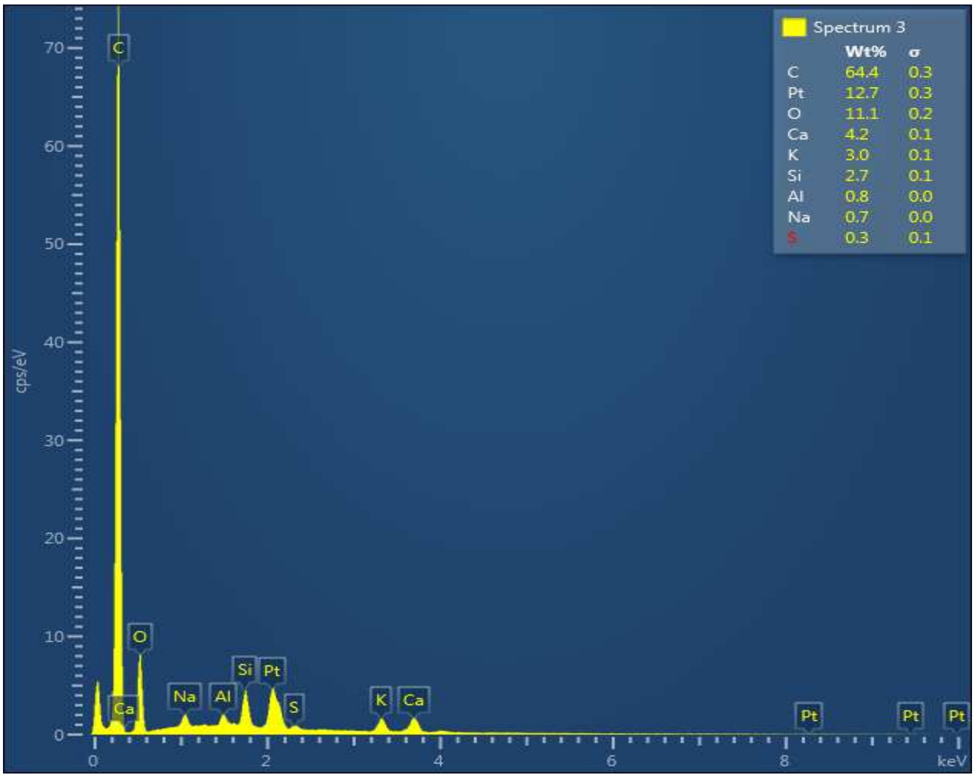

(b)

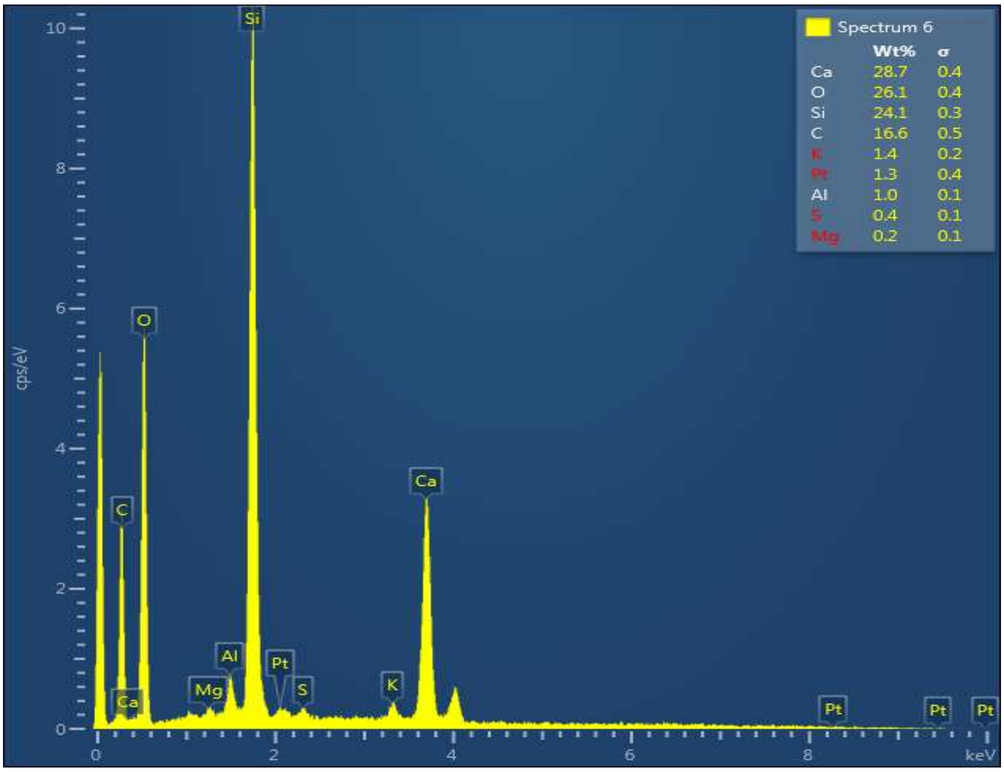

(c)

Figure 8 SEM images and EDS analysis on sample D1 (a) Bundled fiber imaged from SEM (b) The EDS result for spot 1 (c) The EDS result for spot 2

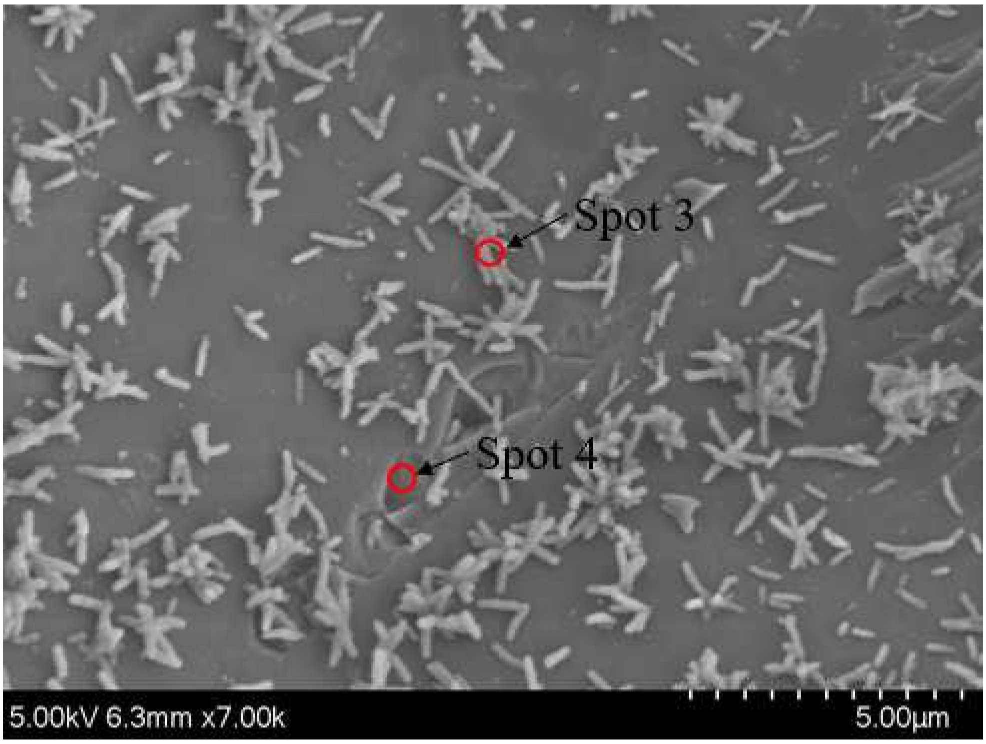
Spot 3
Spot 4
5.00kV 6.3mm x7.00k
5.00μm

(a)

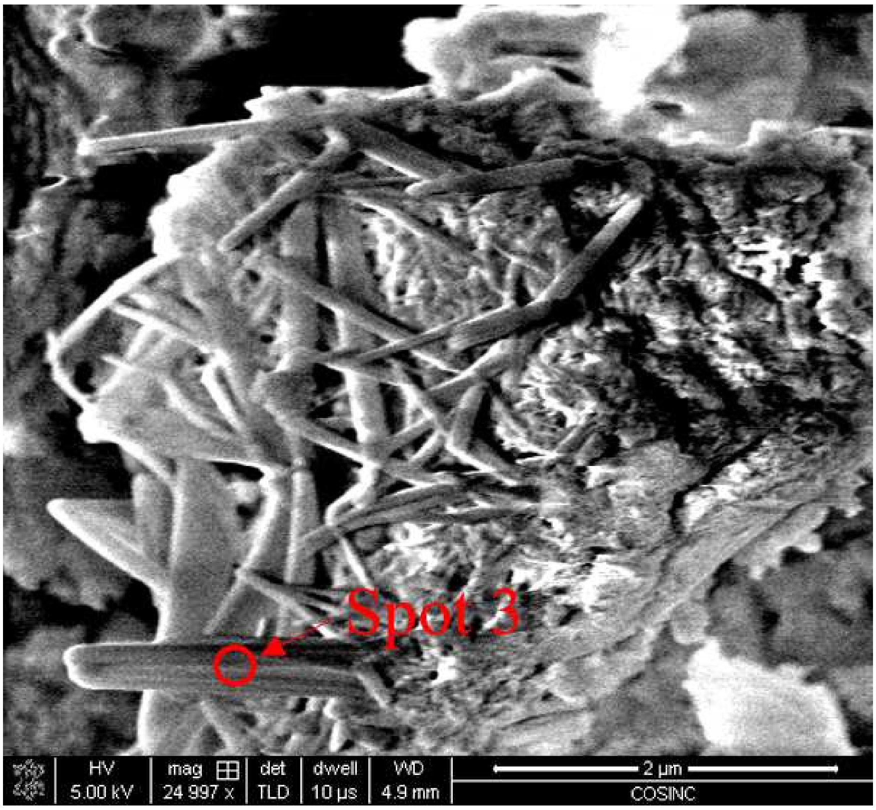
Spot 3
HV
5.00 kV
mag
24 997 x
det
TLD
dwell
10 μs
WD
4.9 mm
2 μm
COSINC

(b)


Spot 4
HV
10.00 kV
mag
19 980 x
det
TLD
dwell
30 µs
WD
5.0 mm
3 µm
COSINC

(c)

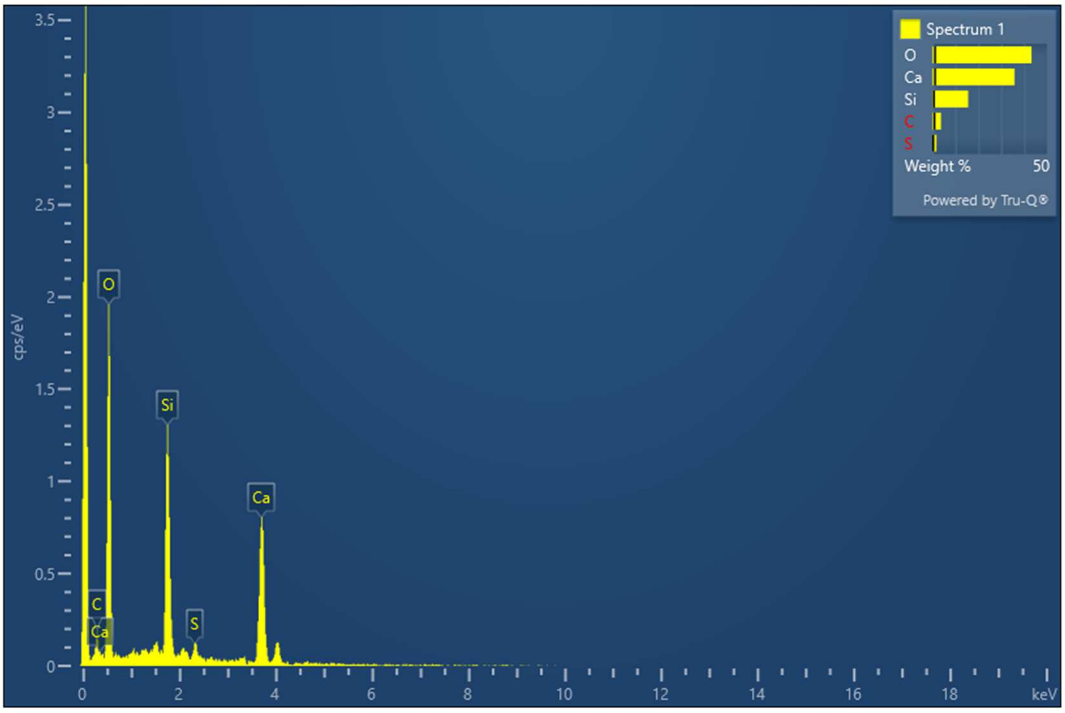
Spectrum 1
O
Ca
Si
C
S
Weight %
50
Powered by Tru-Q®
cps/eV
3.5
3
2.5
2
1.5
1
0.5
0
O
Si
Ca
C
Ca
S
0
2
4
6
8
10
12
14
16
18
keV

(d)

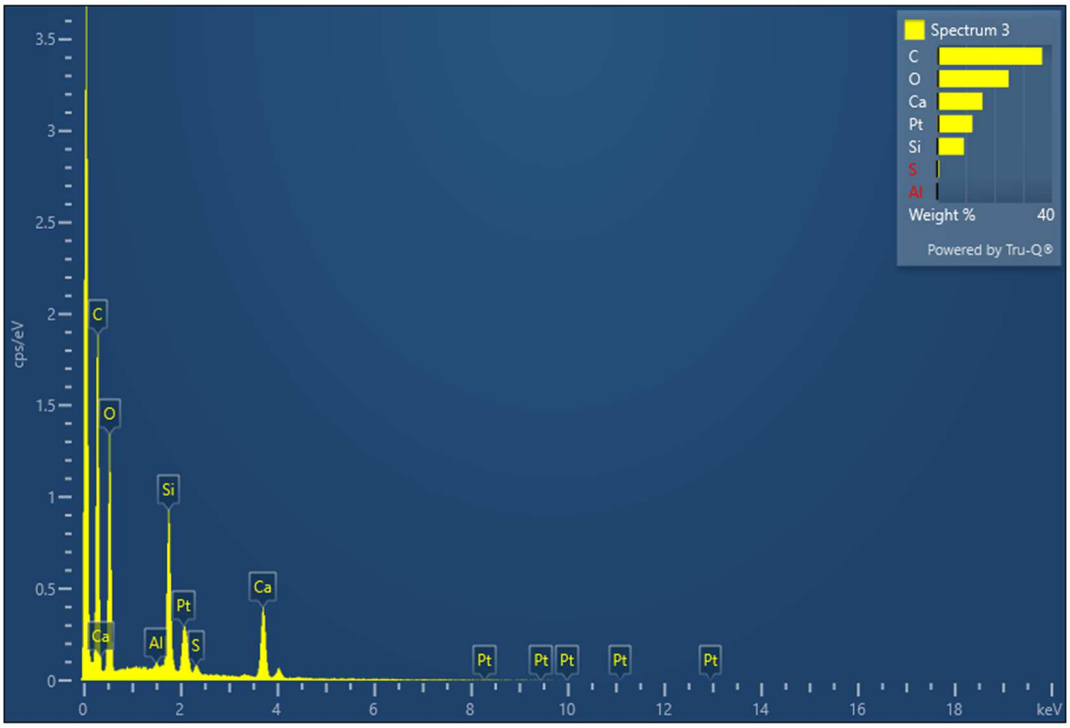

(e)

Figure 9 SEM images and EDS analysis on sample D10 (a) Large scale SEM image on sample D10 (b) Needle-shaped product imaged from FIB-FESEM (spot 1 in Fig. 9 a) (c) Single fiber imaged from FIB-FESEM (spot 2 in Fig. 9 a) (d) The EDS result for spot 3 (e) The EDS result for spot 4

4.2.2 *Sensitivity analysis*

The optimal ultrasonic dispersion times are presented based on the results from porosity measurements and flexural tests, shown in Fig. 10. T4, with 10 mins of ultrasonic dispersion time, delivered the lowest porosity, the highest flexural stress, strain, and toughness. A clear trend for porosity and flexural performance are captured. The smaller the ultrasonic dispersion energies applied, the larger porosity and the higher flexural performance for UHPC-CNFs is achieved. Dispersion times longer than 10 mins was not considered because of the potential evaporation of liquid due to the associated temperature increase. After long-term dispersion, the ultrasonic probe generates heat and further transferred the heat to the dispersion liquid.

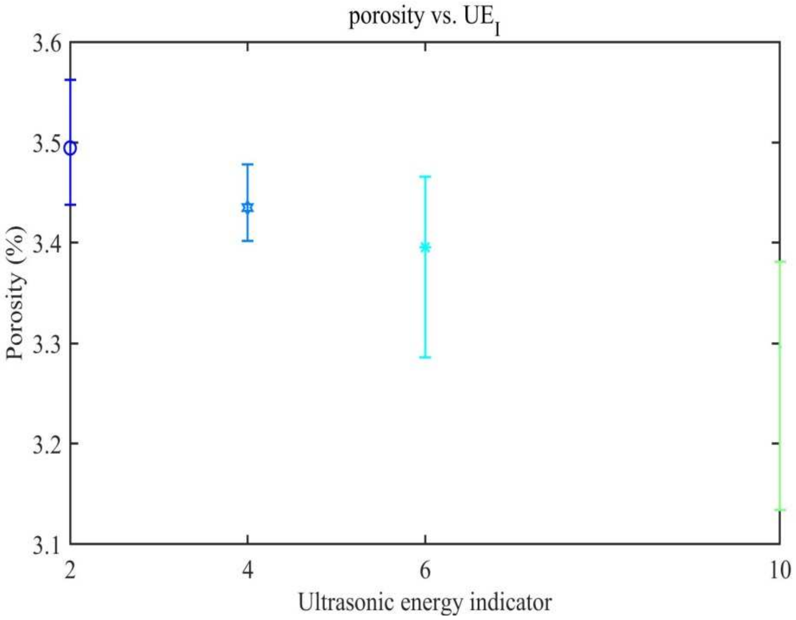
porosity vs. UE_I
Porosity (%)
3.6
3.5
3.4
3.3
3.2
3.1
2
4
6
10
Ultrasonic energy indicator

(a)

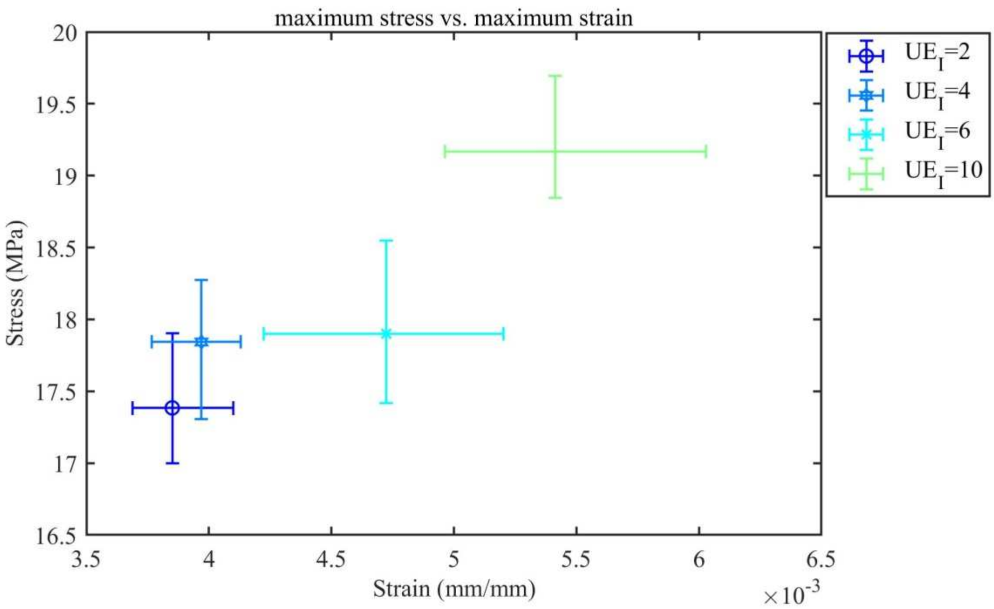
maximum stress vs. maximum strain
UE_I=2
UE_I=4
UE_I=6
UE_I=10
Stress (MPa)
20
19.5
19
18.5
18
17.5
17
16.5
3.5
4
4.5
5
5.5
6
6.5
Strain (mm/mm)
$\times 10^{-3}$

(b)

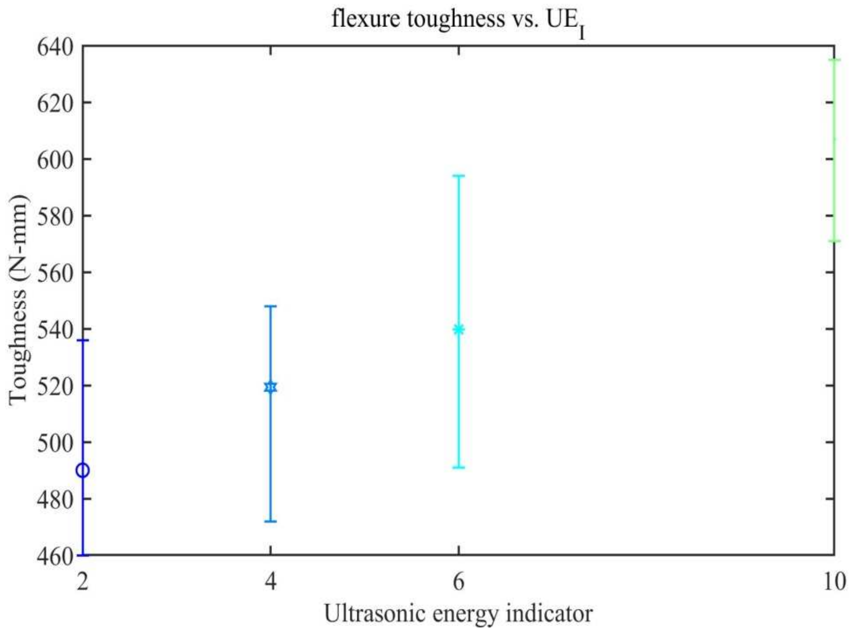

(c)

Notes: The testing results were analyzed from the average value of three identical samples and the error bar provided in the figure offered the minimum and maximum value of the testing results.

Figure 10 UHPC-CNFs from different ultrasonic dispersion energies delivered in dispersion (a) porosity measuring (b) maximum stress vs. maximum strain from flexure test (c) flexure toughness

The dosage and proportion of HRWR in the dispersion liquid was researched and the results are reported in Fig. 11. By increasing the proportion of HRWR used in dispersion from 5:1 to 10:1 (from H1 to H2), the porosity was increased to a small extent, and the maximum flexural strain was increased by around 15% with a slight decrease of the maximum flexural stress. The flexural toughness, increased from 607 N-mm to 610 N-mm. By controlling the total amount of CNFs in the mix, the larger proportion of HRWR applied in dispersion process, technically could have a better dispersion of CNFs. To understand the ultrasonic dispersion-HRWR mechanism behind the phenomenon, further study needs to be done. On the other hand, by increasing the total amount of HRWR used in mixing (H5-H8), the porosity increased, and the flexural performance decreased, especially the maximum flexural strain, which dropped around 8-12%. This is because the extra added HRWR in the mix could retard the hydration process and increase the porosity, which is not beneficial. Through the addition of methylcellulose in dispersion, the flexural strain was further increased in a limited manner with a large drop of flexural stress and flexural toughness.

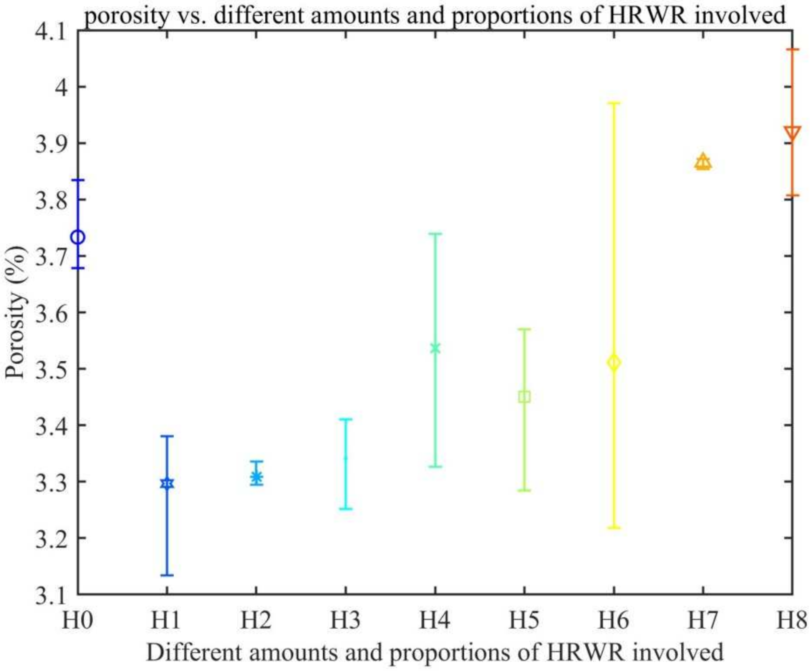
porosity vs. different amounts and proportions of HRWR involved
Porosity (%)
4.1
4
3.9
3.8
3.7
3.6
3.5
3.4
3.3
3.2
3.1
H0
H1
H2
H3
H4
H5
H6
H7
H8
Different amounts and proportions of HRWR involved

(a)

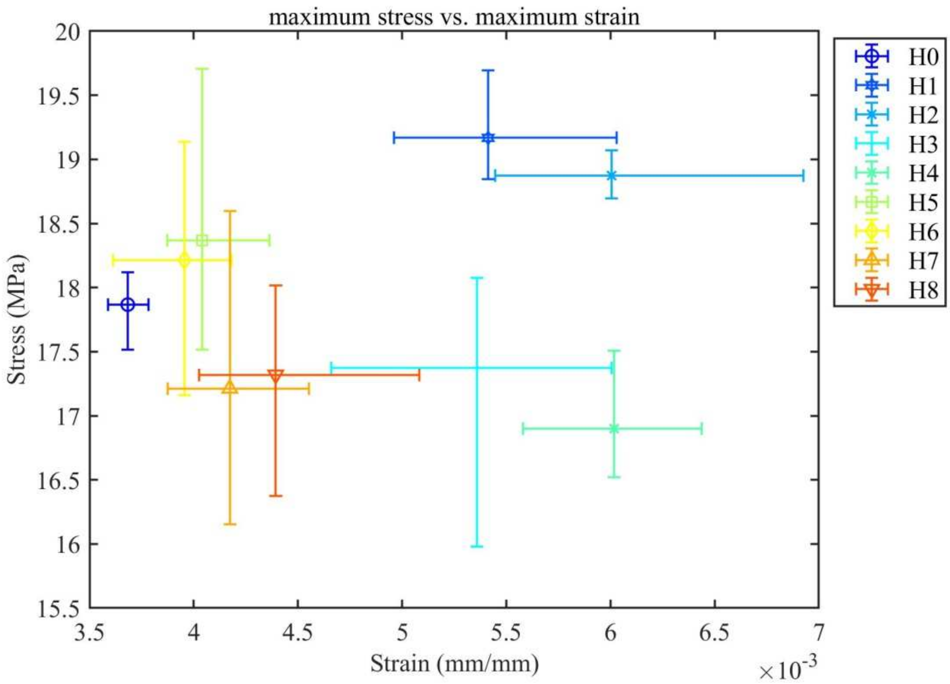
maximum stress vs. maximum strain
Stress (MPa)
20
19.5
19
18.5
18
17.5
17
16.5
16
15.5
3.5
4
4.5
5
5.5
6
6.5
7
Strain (mm/mm)
×10^-3
H0
H1
H2
H3
H4
H5
H6
H7
H8

(b)

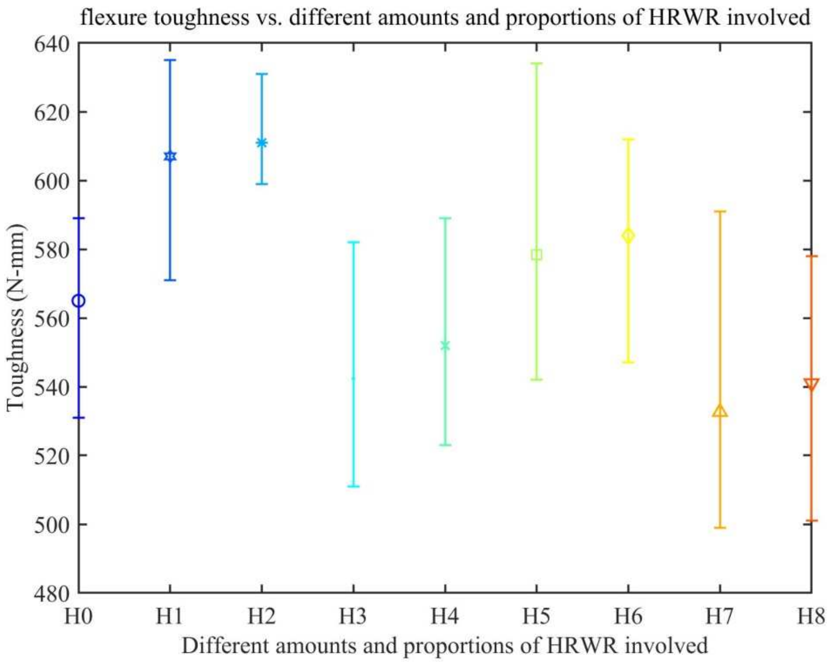

(c)

Notes: The testing results were analyzed from the average value of three identical samples and the error bar provided in the figure offered the minimum and maximum value of the testing results.

Figure 11 UHPC-CNFs from different amount and proportions of HRWR involved in dispersion (a) porosity measuring (b) maximum stress vs. maximum strain from flexure test (c) flexure toughness

The optimal dosage of CNFs added in UHPC is investigated and presented in Fig. 12 with porosity measurements and flexural performance. The lowest porosity and highest flexural performance were delivered by prism samples with 0.1 cwt% of CNFs. With additions of CNFs over 0.1 cwt%, the maximum flexural stress, maximum flexural strain, and flexural toughness were not increased, but decreased. This is because the most effective dispersion technique presented in the last section cannot deliver a homogenous distribution of CNFs beyond the 0.1 cwt% in the cement matrix. As a consequence, the inhomogeneous distribution of CNFs may cause the microscale stress concentrations which resulted in the prisms at a lower load capacity.

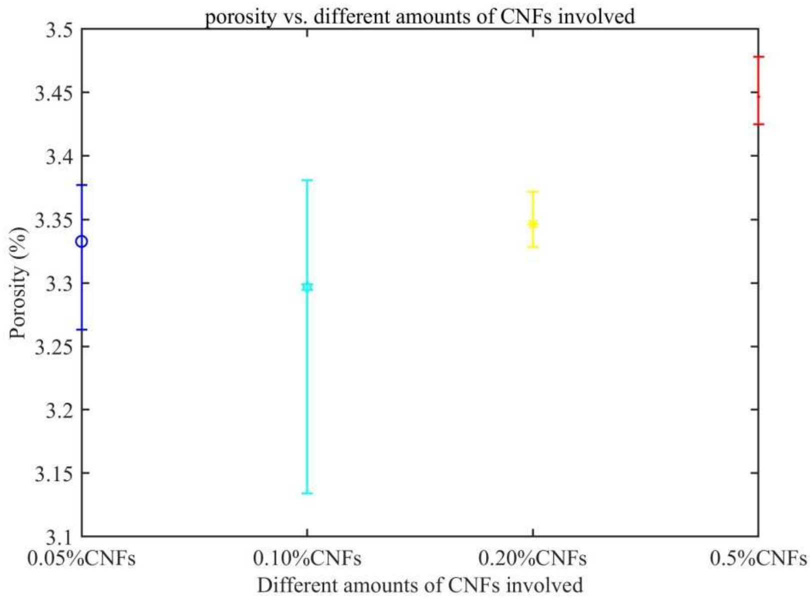
porosity vs. different amounts of CNFs involved
Porosity (%)
3.5
3.45
3.4
3.35
3.3
3.25
3.2
3.15
3.1
0.05%CNFs
0.10%CNFs
0.20%CNFs
0.5%CNFs
Different amounts of CNFs involved

(a)

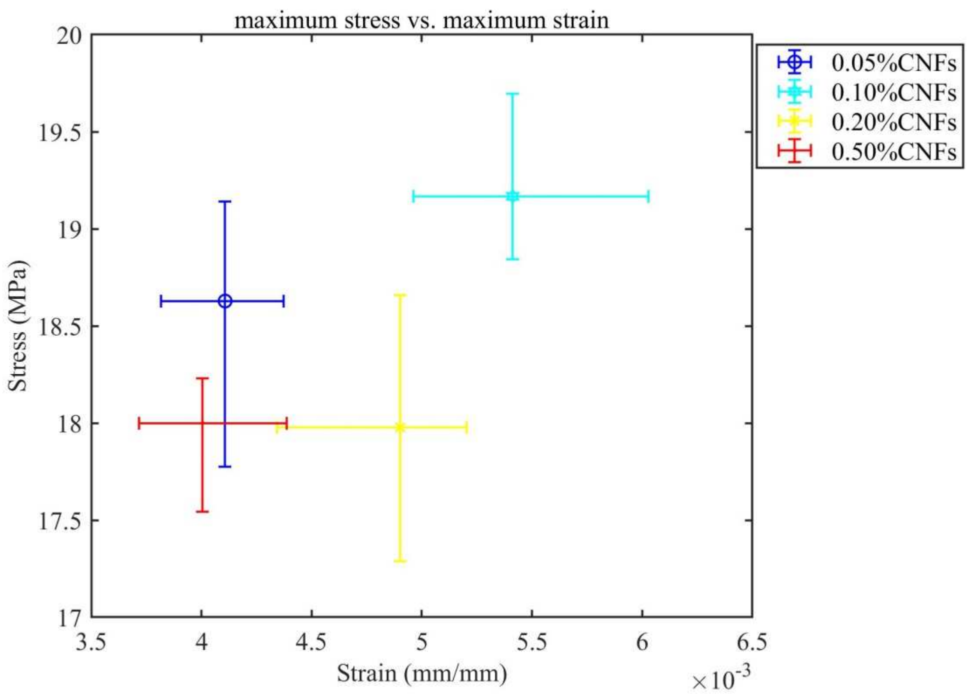
maximum stress vs. maximum strain
0.05%CNFs
0.10%CNFs
0.20%CNFs
0.50%CNFs
Stress (MPa)
20
19.5
19
18.5
18
17.5
17
3.5
4
4.5
5
5.5
6
6.5
Strain (mm/mm)
×10^-3

(b)

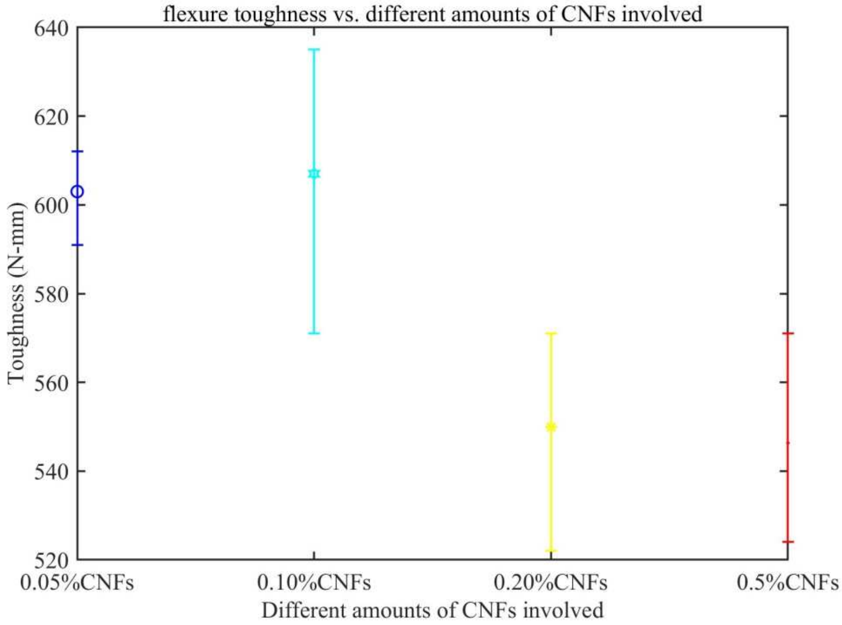

(c)

Notes: The testing results were analyzed from the average value of three identical samples and the error bar provided in the figure offered the minimum and maximum value of the testing results.

Figure 12 UHPC-CNFs from different amounts of CNFs involved (a) porosity measuring (b) maximum stress vs. maximum strain from flexure test (c) flexure toughness

To investigate the effect of the size of fine aggregate applied in UHPC-CNFs, porosity measurements and flexural tests were conducted on samples with screened sand on #16 sieves (F1-F3) and screened sand on #60 sand (F4-F6). The lower porosity and higher flexural performance were achieved by samples with finer sand. The finer sand doesn't only contribute to a higher packing density of UHPC-CNFs composites, but also provides higher friction during the mixing that can aid the dispersion of CNFs. In addition, the application of the most effective dispersion technique, D10, proved to be commonly valid for UHPC-CNFs composites with different sizes of fine aggregate.

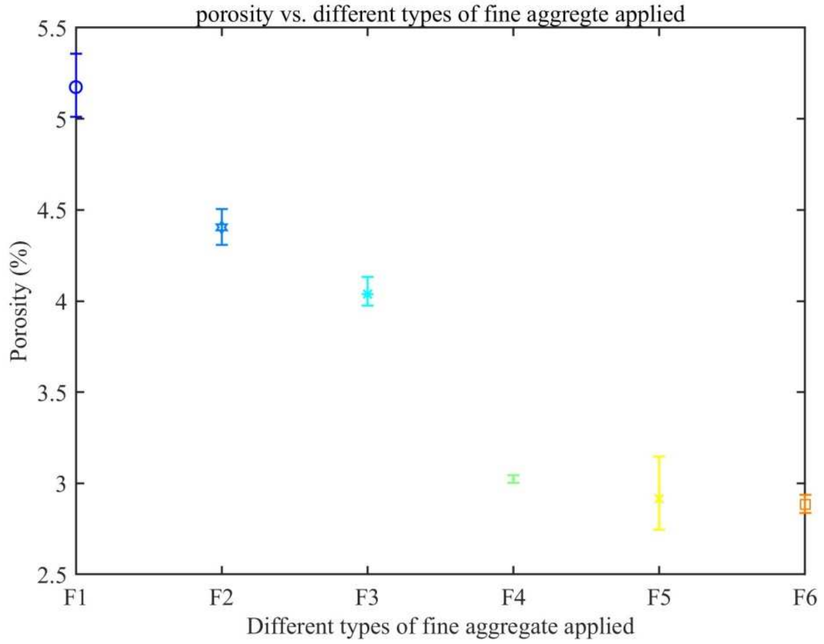
porosity vs. different types of fine aggregte applied
Porosity (%)
5.5
5
4.5
4
3.5
3
2.5
F1
F2
F3
F4
F5
F6
Different types of fine aggregate applied

(a)

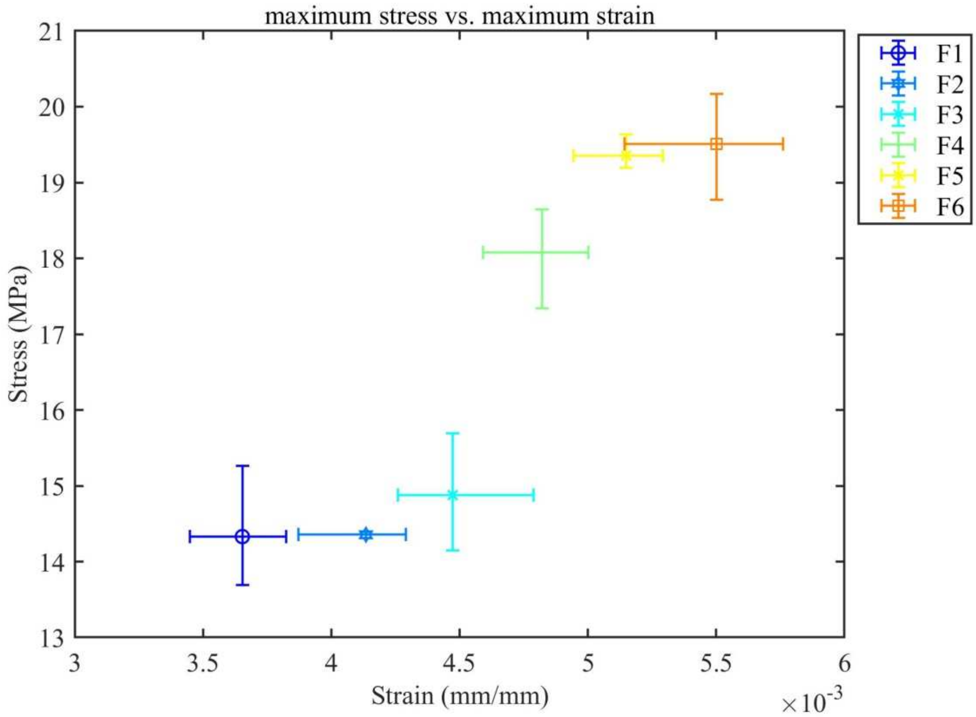
maximum stress vs. maximum strain
Stress (MPa)
21
20
19
18
17
16
15
14
13
3
3.5
4
4.5
5
5.5
6
Strain (mm/mm)
$\times 10^{-3}$
F1
F2
F3
F4
F5
F6

(b)

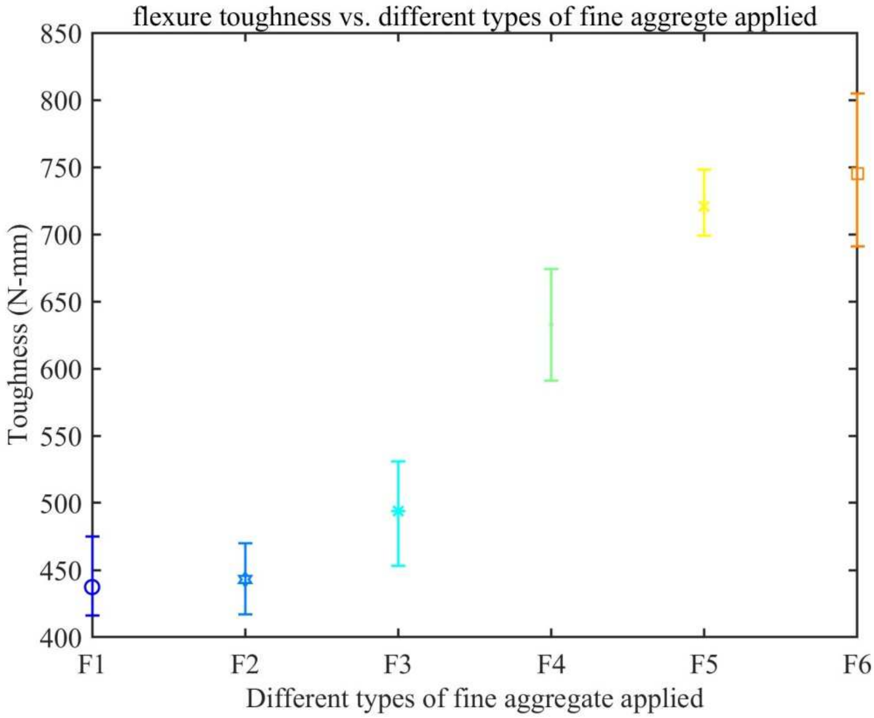

(c)

Notes: The testing results were analyzed from the average value of three identical samples and the error bar provided in the figure offered the minimum and maximum value of the testing results.

Figure 13 UHPC-CNFs from different types of fine aggregate applied (a) porosity measuring (b) maximum stress vs. maximum strain from flexure test (c) flexure toughness

In summary, it can be concluded that with the most effective dispersion technique applied, the optimal ultrasonic dispersion time was confirmed as 10 mins. The proportion of HRWR used for dispersion selected such that 5 parts of HRWR provided the maximum stress, and 10 parts of HRWR provided the maximum strain. There was no clear trend observed between the flexural toughness and the amount of HRWR involved in dispersion. In addition, the addition of extra HRWR during the mixing stage caused a detrimental side effect to the UHPC-CNFs composite. The optimal dosage of CNFs adopted in UHPC-CNFs composites were kept as 0.1 cwt%. Adding more CNFs can deliver an inhomogeneous distribution given the current maximum HRWR. The introduction of finer sand helped to improve the packing density of UHPC-CNFs composites and provided a good dispersion of CNFs in the matrix.

4.3 Mechanical properties

4.3.1 Compressive strength of UHPC-CNFs cylinders

The compressive strength of three groups of cylinders cured for 7/28 days is shown in Fig. 14. From 7 days of curing to 28 days of curing, the averaged compressive strength increased by 18%. A similar trend is obtained from different curing conditions. C2 achieved the largest compressive strength and C3 delivered the lowest compressive strength. When compared with the C1 samples without CNFs, the averaged compressive strength of samples with CNFs for C2 samples are about 2% for 7 days curing and 2.5% for 28 days curing, respectively. With more HRWR applied for CNF dispersion, the averaged compressive strength of C3 is lower than the averaged compressive strength of C1 samples with a 2% decrease. By considering the deviation of compressive strength among samples from the same group, it can be concluded that the compressive strength of UHPC is not effectively improved with the addition of well-dispersed CNFs. These is no significant change in compressive strength for this addition of random nanomaterials. It is noticed that from composite mechanics theory, adding nano-level inert fillers, such as CNFs, can tremendously improve the mechanical behavior (e.g., compressive strength) because of their remarkable mechanical properties. The added inert fillers can fill the porous media and cracks left from either the hydration process or the defects. However, in reality, simply using the composite mechanics formulations to predict the compressive strength is not applicable because other factors, such as the workability, the bonding strength between different compositions are not considered. The improvement of adding nanomaterials in cementitious materials is limited and cannot be anticipated from the theory [71, 72].

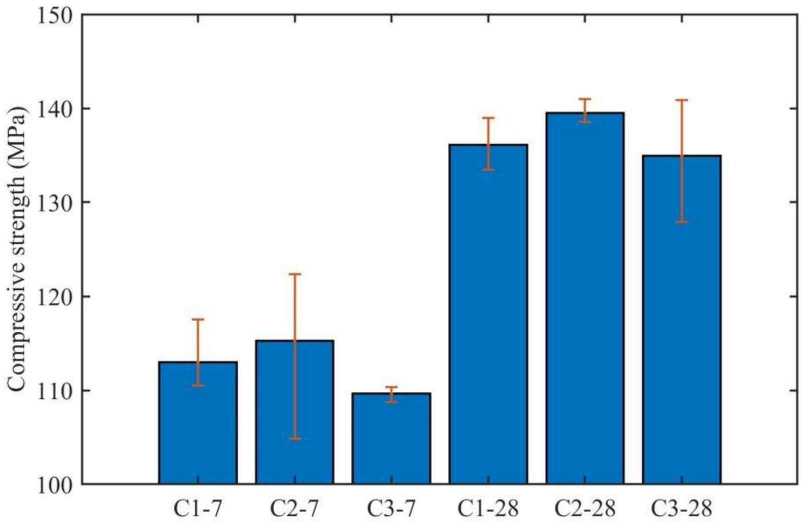

Notes: The testing results were analyzed from the average value of three identical samples and the error bar provided in the figure offered the minimum and maximum value of the testing results.

Figure 14 Compressive strength of UHPC-CNFs cylinders with different curing time

4.3.2 *Flexural properties of UHPC-CNFs prisms*

The change in flexural properties with the addition of CNFs in UHPC is reported in Fig. 15. The maximum stress collected from the flexure test is improved around 10% from 7 days of curing to 28 days of curing. A large increase of maximum strain can be found for C1 samples from 7 days of curing to 28 days of curing, equaling 29%. However, long-term curing does not improve the maximum strain for samples with CNFs. Comparing the results among different groups, the maximum strain and the largest flexure toughness are seen in C3 with 28 days of curing, and the maximum stress is from C2 with 28 days of curing. Compared to the reference samples C1, the magnitude of the improvement can go up to 7.4% of maximum flexural stress and 63% of maximum flexural strain, respectively. These improvements are attributed to the high tensile performance of CNFs. With a good dispersion of CNFs in UHPC, the functionality of CNFs in UHPC-CNFs composites can be maximized. From a fracture mechanics point of view, the input of CNFs in UHPC is not only acted as the bridging effect after the cracks appeared, but also provided the elongated shape that can cause the cracks to travel further around these stiff inclusions.

In summary, the introduction of well-dispersed CNFs in UHPC can help to improve the flexural properties from maximum stress, maximum strain, and flexure toughness. With additional HRWR used during the CNFs dispersion (C3), a larger improvement of the capability of deformation can be achieved. On the other side, the more HRWR involved in CNFs dispersion could cause a lower peak load.

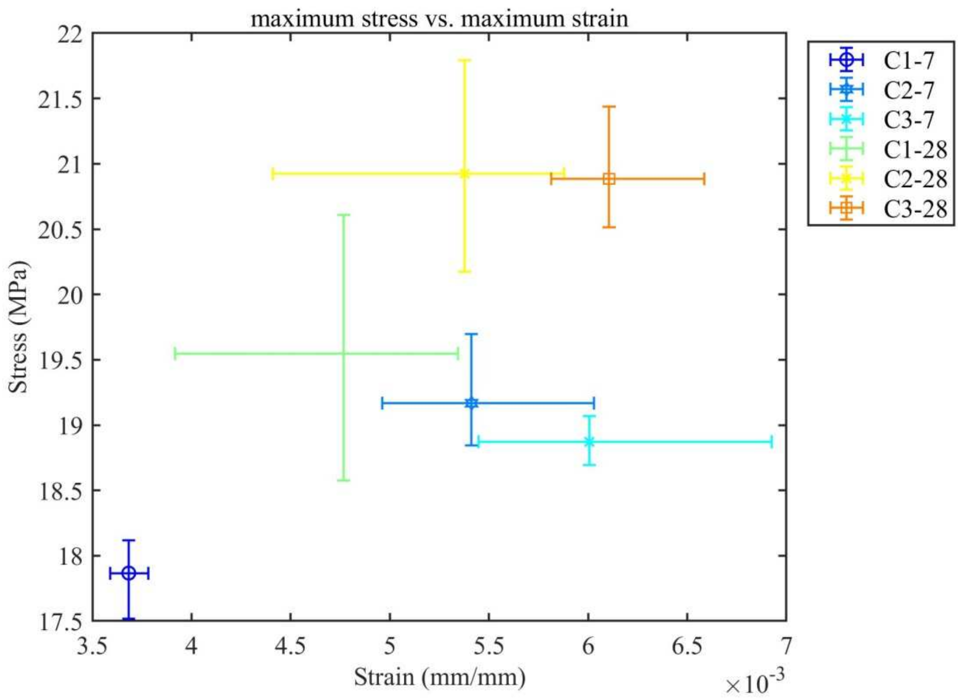

(a)

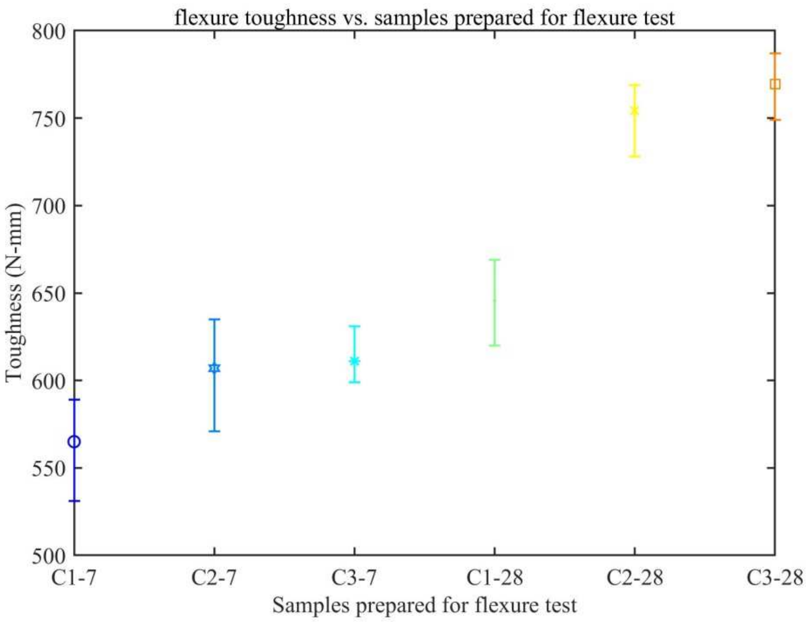

(b)

Notes: The testing results were analyzed from the average value of three identical samples and the error bar provided in the figure offered the minimum and maximum value of the testing results.

Figure 15 Flexural properties of UHPC-CNFs composites with different curing time (a) maximum stress vs. maximum strain (b) flexure toughness

4.4 Workability

4.4.1 *Slump of UHPC-CNFs slurry*

The slump test results from the UHPC without CNFs, and the two UHPC-CNF composites with the most effective dispersion methods applied are provided in Fig. 16. By adding the CNFs, a decrease of the slump of the slurry is visible, especially for C2, which provided a 10.5% slump drop. This increase of viscosity can be attributed to the large surface area of CNFs. The water adsorption of the mix can be enhanced when high surface area materials are added. Since the CNFs surface property was changed from hydrophobic to hydrophilic during dispersion, the water ions were attracted and stayed at the surface of CNFs, which also caused a decrease of slurry fluidity.

In addition, the increase of the amount of HRWR in the CNFs dispersion can increase the relative fluidity of the slurry by about 5%. Because the total amount of HRWR and CNFs used in C2 and C3 are kept constant, it can be concluded that the functionality of the part of HRWR used for CNFs dispersion is not weakened but enhanced. From the dispersion point of view, it can be analyzed that the main reason the functionality of HRWR can be enhanced is because of the increment of the surface activity of HRWR, which was enforced during ultrasonic dispersion.

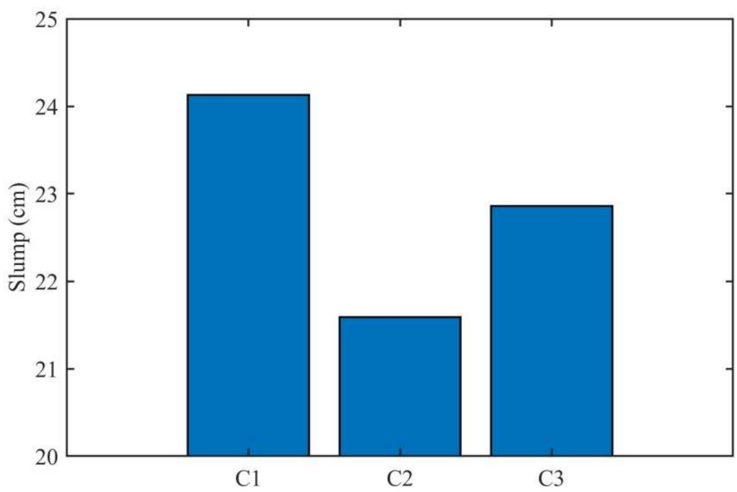

Figure 16 Slump of UHPC-CNFs composites

4.4.2 *Temperature evolution of UHPC-CNFs composites*

To reveal the effect of adding CNFs on the temperature evolution of UHPC, the temperature evolution measurement which captures the temperature change during the hydration process, was done and the results as compared to the UHPC mixture (C1) are reported in Fig. 17. It can be seen that the addition of CNFs in UHPC can effectively decrease the peak temperature that can be achieved. Comparing the total temperature evolution to C1, the samples with CNFs show an 8.3% decrease for C2 and an 18.2% decrease for C3. Corresponding to the maximum hydration heat, the evolution of the temperature is similar in the peak position. There is some prolonged hydration for C2 in the descending branch of Fig.17. This minimized retardation would cause marginal effects on the construction of UHPC-CNFs composites onsite.

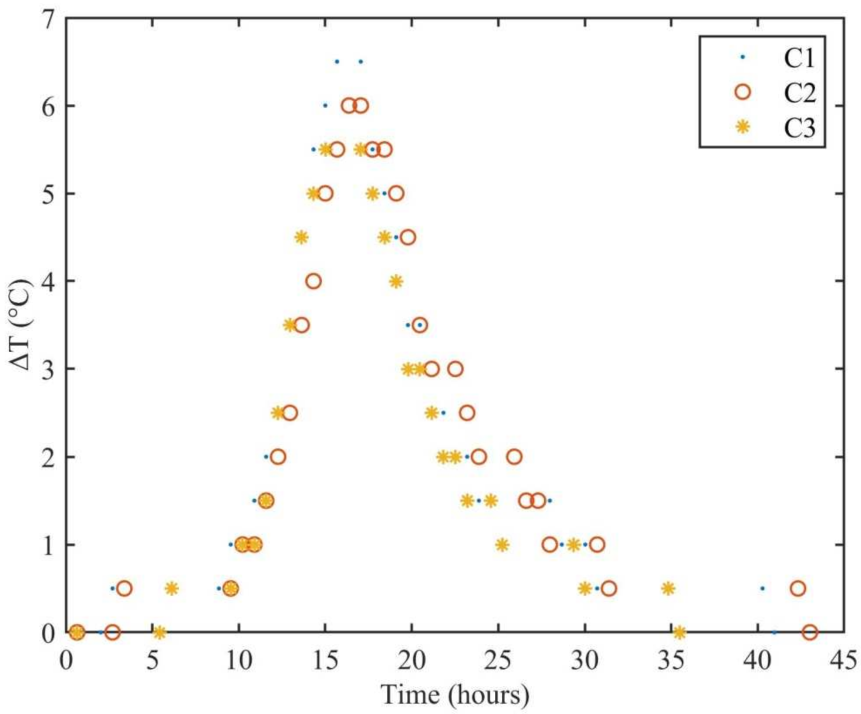

Figure 17 Temperature change of UHPC-CNFs composites during the hydration phase

4.5 Permeability

4.5.1 *Water permeability of UHPC-CNFs composites*

Fig. 18 shows the relative mass change of samples by absorbing water from the bottom edge of sealed cylinder samples for 216 hours. It can be seen from the results that adding well-dispersed CNFs effectively inhibits the water uptake into the UHPC material. Compared to the reference C1, the relative mass change of samples after the wicking test is decreased 18% for C2 and 11% for C3. The major differences of mass change were generated in the first 24 hours. After that, a similar slope of increment of the mass change for all groups was obtained. From the figure, the lowest water permeability of UHPC-CNFs can be defined as the smallest relative mass change during the wicking test, which is C2. Compare with C3, C2 samples have less HRWR involved in the CNFs dispersion, which caused lower porosity. Therefore, the relation between sample porosity and water permeability holds for UHPC-CNF composites.

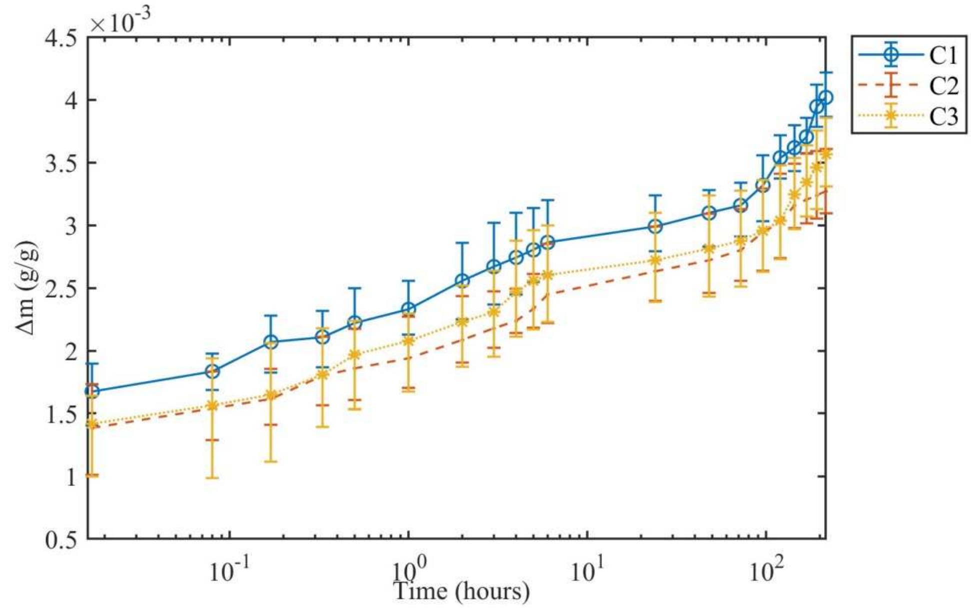

Notes: The testing results were analyzed from the average value of three identical samples and the error bar provided in the figure offered the minimum and maximum value of the testing results.

Figure 18 Mass change of UHPC-CNFs composites during the wicking test

4.5.2 *Chloride permeability of UHPC-CNFs composites*

The ponding test was conducted on three different groups of samples. The 1-month and 3-month ponding results are reported in Fig. 19 (a) and (b), respectively. Each chloride profile is from the average results of three identical samples. The same trend can be found from both figures that the UHPC-CNF composites (C2 and C3) provided lower chloride concentrations compare to the pure UHPC (C1), especially on the tops of the samples, which are close to the source of chloride. This means the chloride resistance can be improved for UHPC with well-dispersed CNFs.

From Fig. 19 (a), the concentrations of acid-soluble chloride ions at 0-12.7 mm are 0.0233 cwt% for C1 to 0.017333 cwt% for C2, and 0.02 cwt% for C3, which presented chloride concentration a 25.7% decrease from C1 to C2 and a 14.3% decrease from C1 to C3 in the surface layers. In the deep layers (over 40 mm), the chloride concentration was not able to be captured due to the short-term ponding. From the results of 3-month ponding, relatively closer concertation of chloride ions can be found from the surface layers because an equilibrium concentration was achieved. On the other side, a consistent decrease in the concentration of chloride ions can be found from other depths (over 10 mm), which means more chloride ions did penetrate the deep layers and the functionality of chloride resistance from CNFs is more clearly captured. In addition, because of the larger proportion of HRWR involved in dispersion, a lesser chloride permeability is shown in C2. This consistent trend can also be found in porosity measurements and water permeability measurements. The comparison between 1-month ponding and 3-month ponding shows that with two extra months of the ponding process, the averaged chloride concentrations at different depths are increased 236% from C1, 226% from C2, and 202% from C3. Both C2 and C3 provided lower increment of chloride concentrations after the extra 2-month of ponding process compared to samples without CNFs (C1), which further proved the improvement of chloride resistance due to the addition of CNFs.

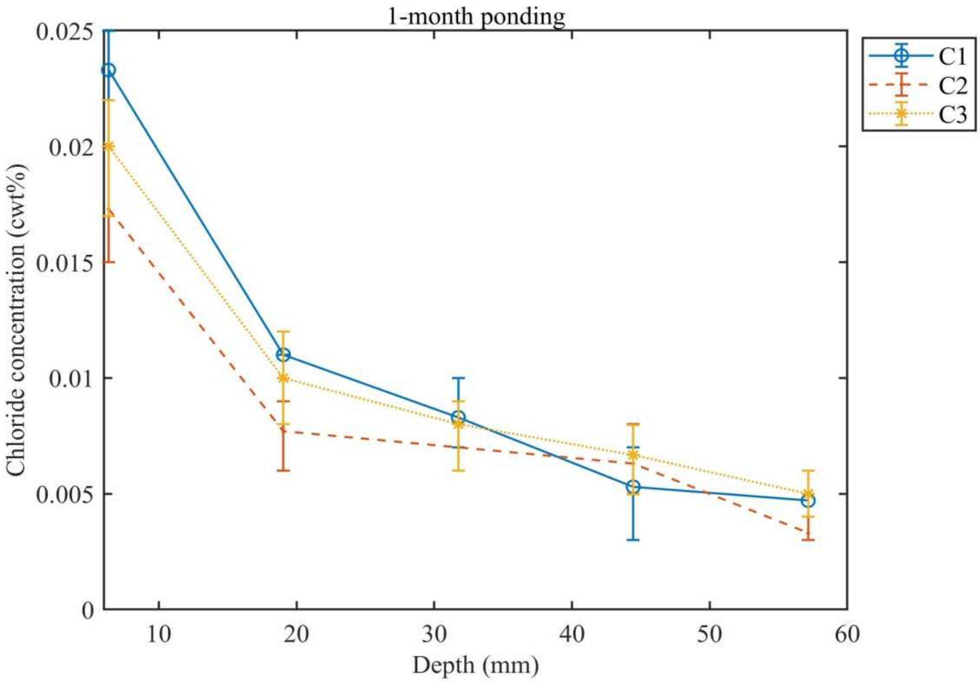

(a)

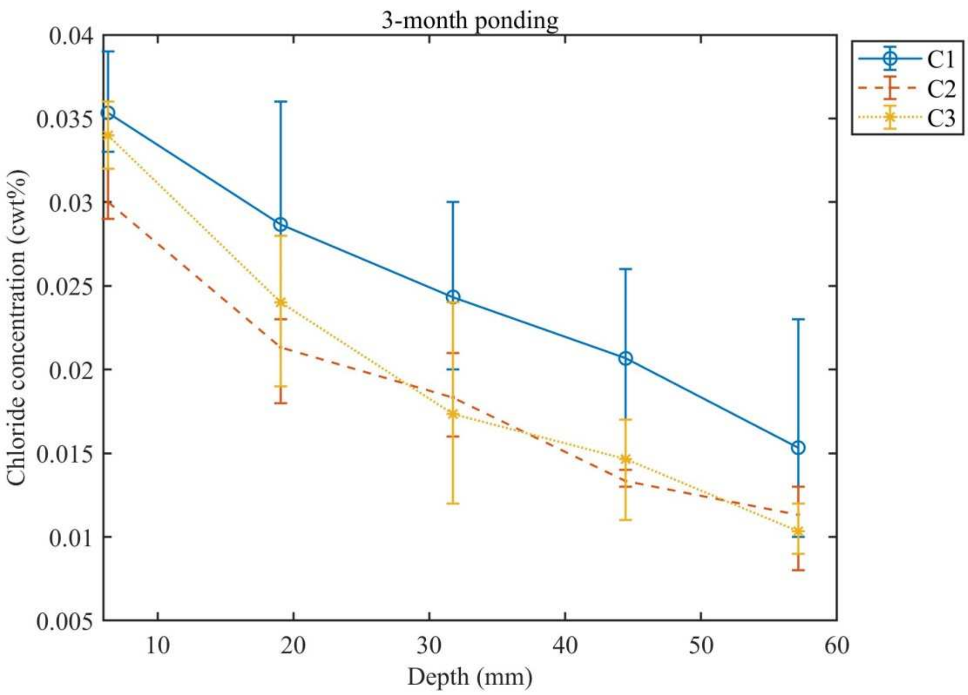

(b)

Notes: The testing results were analyzed from the average value of three identical samples and the error bar provided in the figure offered the minimum and maximum value of the testing results. The unit of cwt% is the amount of Cl per cement.

Figure 19 Average chloride profile of UHPC-CNFs composites in (a) 1-month ponding (b) 3-month ponding

5 Discussion

The application of finer sand caused a lower porosity and higher flexural toughness of the UHPC-CNFs composite (Fig. 13), which provided a more dominated role than the effect of CNFs. This means providing a denser material with strong flexural toughness has to be considered at different scales, not only at the nanoscale, but also the microscale and macroscale. Due to the limited amount of CNF added, the contribution of CNFs in UHPC was severely restricted. Alternatively, more HRWR may enable higher CNF concentrations. However, the requirements of the HRWR in the UHPC mix seem to be the limiting factor preventing the dispersion of additional CNFs. This means for UHPC mix design, selecting the size of fine sand becomes more important in delivering a strong, and durable material and should be emphasized in the future research.

Note that the results provided from the temperature evolution measurement (Fig. 17) are opposite to the prediction from classic nucleation theory [73]. According to nucleation theory, the CNFs applied in UHPC mix design could act as seeds and accelerate the temperature change. Based on the testing results, it can be assumed that while the increased surface area can govern the hydration reaction rate in classic nucleation theory, in this mix the temperature evolution is dominated by other factors, such as the effects of the HRWR. The introduction of HRWR in cementitious material can delay the hydration process. During the ultrasonication, it is questionable that the chemical structure of HRWR was altered, and the functionality was further enhanced [74], which provided a higher impact on the temperature evolution than the nucleation effect. Therefore, further investigation should be conducted to prove the coupling effect of nucleation and HRWR retardation to the hydration process by a more precise test, such as the calorimetry test.

In view of the results provided in section 4.2, applying an effective dispersion technique can improve the contribution of CNFs applied in UHPC by delivering a more uniform distribution of CNFs. In previous published works [18-43], inconsistent dispersion techniques were applied in each research study and there is no direct comparison provided among them. By comparison of the different dispersion techniques, the agglomerated bundles of CNFs can be most effectively eliminated from the cementitious material. With a uniform distribution of CNFs in UHPC achieved by the most effective dispersion technique, a comprehensive enhancement of UHPC can be found not only in mechanical properties, but also in resistance of permeability. It can be expected in the future that the newly developed dispersion technique could be applied to deliver a uniform liquid form of CNFs, and further this liquid form can be mixed with other UHPC ingredients (sand, cement) in the field with minimum retardation of cement hydration process.

6 Summary and conclusions

A comprehensive study of UHPC-CNFs composites was experimentally conducted step-by-step regarding the selection of UHPC mix design, the CNF dispersion method, and the following mechanical properties, workability, and permeabilities of UHPC-CNF composites. The optimal UHPC mix design was obtained with the lowest w/c ratio and all-purpose natural sand, which provided the highest compressive strength under different curing conditions and the largest slump.

Starting from the optimal UHPC mixture, a good dispersion of CNFs in UHPC was shown in reference to improved flexural behavior and porosity; and verified by SEM analysis. HRWR was selected as the most effective chemical surfactant to be used for CNFs dispersion. Macroscale dispersion (magnetic stirring) followed by microscale dispersion (ultrasonic dispersion) was found to be the most efficient technique to disperse CNFs in UHPC. It is noted that an effective dispersion technique can tremendously affect the functionality of CNFs. Multiple factors were involved in this process, such as the selection of chemical surfactants, the duration of ultrasonic dispersion, etc. The following sensitivity analysis was then further provided to determine the optimal ultrasonic dispersion parameters. From the analysis, the ultrasonic energy indicator (UE_I) equals 10; the proportion of HRWR applied for CNFs dispersion are from 5-10 times more than the amounts of CNFs, which depends on either the high stress or the high strain achieved; the 0.1 cwt% CNFs dosages was selected with the largest flexural performance delivered.

The effectiveness of adding CNFs into UHPC was investigated in the context of mechanical properties, workability, and permeability. By adding CNFs to UHPC, the flexural performance can be dramatically raised. The maximum flexural stress and maximum flexural strain can be increased up to 7.3% and 63%, respectively. Similarly, the water permeability and chloride permeability can be decreased with the addition of well-dispersed CNFs. On the other side, the slump was decreased up to 10%. Increasing the amount of HRWR involved in the dispersion can mitigate the drop of the slump. In addition, a limited retardation of the hydration process was found with CNFs added from the temperature evolution measurement. Due to the limitation of the temperature evolution measurement, a more precise method, such as the isothermal calorimetry test, is preferred for further investigation.

CRediT authorship contribution statement

Linfei Li: Investigation, Writing – original draft. **Boning Wang:** Writing – review & editing. **Mija H. Hubler:** Writing – review & editing, Supervision, Funding acquisition.

Declaration of competing interest

The authors declare that they have no know competing financial interests or personal relationships that could have appeared to influence the work reported in this paper.

Acknowledgment

Financial support of the U.S. Department of Energy (project Modular Processing of Flare Gas for Carbon Nanoproducts, DE-FE0031870) is gratefully acknowledged.

References

[1] D.M. Roy, G.R. Gouda, A. Bobrowsky, Very high strength cement pastes prepared by hot pressing and other high pressure techniques, Cem. Concr. Res. 2 (1972) 349–366. doi:https://doi.org/10.1016/0008-8846(72)90075-0.

[2] J.D. Birchall, A.J. Howard, K. Kendall, Flexural strength and porosity of cements, Nature 289 (5796) (1981) 388-390. doi: https://doi.org/10.1038/289388a0.

[3] D.R. Lankard and J.K. Newell, Preparation of Highly Reinforced Steel Fiber Reinforced Concrete Composites, ACI Symp. Publ. 81 (n.d.). doi:10.14359/6456.

[4] X. Wang, R. Yu, Q. Song, Z. Shui, Z. Liu, S. Wu, D. Hou, Optimized design of ultra-high performance concrete (UHPC) with a high wet packing density, Cem. Concr. Res. 126 (2019) 105921. doi:https://doi.org/10.1016/j.cemconres.2019.105921.

[5] M. Schleiting, A. Wetzel, P. Krooß, J. Thiemicke, T. Niendorf, B. Middendorf, E. Fehling, Functional microfibre reinforced ultra-high performance concrete (FMF-UHPC), Cem. Concr. Res. 130 (2020) 105993. doi:https://doi.org/10.1016/j.cemconres.2020.105993.

[6] F. de Larrard, T. Sedran, Optimization of ultra-high-performance concrete by the use of a packing model, Cem. Concr. Res. 24 (1994) 997–1009. doi:https://doi.org/10.1016/0008-8846(94)90022-1.

[7] A. Hajiesmaeili, E. Denarié, Capillary flow in UHPFRC with synthetic fibers, under high tensile stresses, Cem. Concr. Res. 143 (2021) 106368. doi:https://doi.org/10.1016/j.cemconres.2021.106368.

[8] FHWA Report, Ultra-High Performance Concrete: A State-of-the-Art Report for the Bridge Community, FHWA-HRT-13-060, June 2013.

[9] J. Provete Vincler, T. Sanchez, V. Turgeon, D. Conciatori, L. Sorelli, A modified accelerated chloride migration tests for UHPC and UHPFRC with PVA and steel fibers, Cem. Concr. Res. 117 (2019) 38–44. doi:https://doi.org/10.1016/j.cemconres.2018.12.006.

[10] W. Wang, J. Liu, F. Agostini, C.A. Davy, F. Skoczylas, D. Corvez, Durability of an Ultra High Performance Fiber Reinforced Concrete (UHPFRC) under progressive aging, Cem. Concr. Res. 55 (2014) 1–13. doi:https://doi.org/10.1016/j.cemconres.2013.09.008.

[11] E. Cuenca, L. D'Ambrosio, D. Lizunov, A. Tretjakov, O. Volobujeva, L. Ferrara, Mechanical properties and self-healing capacity of Ultra High Performance Fibre Reinforced Concrete with alumina nano-fibres: Tailoring Ultra High Durability Concrete for aggressive exposure scenarios, Cem. Concr. Compos. 118 (2021) 103956. doi:https://doi.org/10.1016/j.cemconcomp.2021.103956.

[12] C.F. Ferraris, K.H. Obla, R. Hill, The influence of mineral admixtures on the rheology of cement paste and concrete, Cem. Concr. Res. 31 (2001) 245–255. doi:https://doi.org/10.1016/S0008-8846(00)00454-3.

[13] C.K. Park, M.H. Noh, T.H. Park, Rheological properties of cementitious materials containing mineral admixtures, Cem. Concr. Res. 35 (2005) 842–849. doi:https://doi.org/10.1016/j.cemconres.2004.11.002.

[14] R. Siddique, Utilization of silica fume in concrete: Review of hardened properties, Resour. Conserv. Recycl. 55 (2011) 923–932. doi:https://doi.org/10.1016/j.resconrec.2011.06.012.

[15] P.S. Song, S. Hwang, Mechanical properties of high-strength steel fiber-reinforced concrete, Constr. Build. Mater. 18 (2004) 669–673. doi:https://doi.org/10.1016/j.conbuildmat.2004.04.027.

[16] C.X. Qian, P. Stroeven, Development of hybrid polypropylene-steel fibre-reinforced concrete, Cem. Concr. Res. 30 (2000) 63–69. doi:https://doi.org/10.1016/S0008-8846(99)00202-1.

[17] L.R. Betterman, C. Ouyang, S.P. Shah, Fiber-matrix interaction in microfiber-reinforced mortar, Adv. Cem. Based Mater. 2 (1995) 53–61. doi:https://doi.org/10.1016/1065-7355(95)90025-X.

[18] M.S. Konsta-Gdoutos, Z.S. Metaxa, S.P. Shah, Multi-scale mechanical and fracture characteristics and early-age strain capacity of high performance carbon nanotube/cement nanocomposites, Cem. Concr. Compos. 32 (2010) 110–115. doi:https://doi.org/10.1016/j.cemconcomp.2009.10.007.

[19] M.S. Konsta-Gdoutos, Z.S. Metaxa, S.P. Shah, Highly dispersed carbon nanotube reinforced cement based materials, Cem. Concr. Res. 40 (2010) 1052–1059. doi:https://doi.org/10.1016/j.cemconres.2010.02.015.

[20] Y. Li, X. Huang, L. Zeng, R. Li, H. Tian, X. Fu, Y. Wang, W.-H. Zhong, A review of the electrical and mechanical properties of carbon nanofiller-reinforced polymer composites, J. Mater. Sci. 54 (2019) 1036–1076. doi:https://doi.org/10.1007/s10853-018-3006-9.

[21] J. Němeček, L. Li, Y. Xi, Electrokinetic nanoparticle injection for remediating leaks in oil well cement, Constr. Build. Mater. 156 (2017) 63–72. doi:https://doi.org/10.1016/j.conbuildmat.2017.08.152.

[22] W. Tian, Y. Liu, B. Qi, W. Wang, Enhanced effect of carbon nanofibers on heating efficiency of conductive cementitious composites under ohmic heating curing, Cem. Concr. Compos. 117 (2021) 103904. doi:https://doi.org/10.1016/j.cemconcomp.2020.103904.

[23] T. Wang, J. Xu, B. Meng, G. Peng, Experimental study on the effect of carbon nanofiber content on the durability of concrete, Constr. Build. Mater. 250 (2020) 118891. doi:https://doi.org/10.1016/j.conbuildmat.2020.118891.

[24] Z.S. Metaxa, M.S. Konsta-Gdoutos, S.P. Shah, Carbon nanofiber-reinforced cement-based materials, Transportation Research Record 2142 (2010) 114-118. doi:https://doi.org/10.3141/2142-17

[25] R.K. Abu Al-Rub, B. Tyson, A. Yazdanbakhsh, Z. Grasley, Mechanical Properties of Nanocomposite Cement Incorporating Surface-Treated and Untreated Carbon Nanotubes and Carbon Nanofibers, J. Nanomechanics Micromechanics. 2 (2012) 1–6. doi:https://doi.org/10.1061/(ASCE)NM.2153-5477.0000041.

[26] H. Benyahia, M. Tarfaoui, V. Datsyuk, A. El Moumen, S. Trotsenko, S. Reich, Dynamic properties of hybrid composite structures based multiwalled carbon nanotubes, Compos. Sci. Technol. 148 (2017) 70–79. doi:https://doi.org/10.1016/j.compscitech.2017.05.021.

[27] H. Wang, A. Zhang, L. Zhang, Q. Wang, X. Yang, X. Gao, F. Shi, Electrical and piezoresistive properties of carbon nanofiber cement mortar under different temperatures and water contents, Constr. Build. Mater. 265 (2020) 120740. doi:https://doi.org/10.1016/j.conbuildmat.2020.120740.

[28] C.W. Frye, T.R. Rybolt, Nanohashtag structures based on carbon nanotubes and molecular linkers, Surf. Sci. 669 (2018) 34–44. doi:https://doi.org/10.1016/j.susc.2017.11.005.

[29] A. Yazdanbakhsh, Z. Grasley, B. Tyson, R.K. Abu Al-Rub, Distribution of carbon nanofibers and nanotubes in cementitious composites, Journal of the Transportation Research Board 2142 (2010) 89-95. doi:https://doi.org/10.3141/2142-13.

[30] O. Lourie, H.D. Wagner, Transmission electron microscopy observations of fracture of single-wall carbon nanotubes under axial tension, Applied Physics Letters 73(24) (1998) 3527-3529. doi:https://doi.org/10.1063/1.122825.

[31] D.D. Chung, Dispersion of short fibers in cement, J. Mater. Civ. Eng. 17 (2005) 379-383. doi:https://doi.org/10.1061/(ASCE)0899-1561(2005)17:4(379).

[32] C. Chang, G. Song, D. Gao, Y.L. Mo Temperature and mixing effects on electrical resistivity of carbon fiber enhanced concrete, Smart Materials and Structures 22(3) (2013) 035021. doi:https://doi.org/10.1088/0964-1726/22/3/035021.

[33] A. Yazdanbakhsh, Z.C. Grasley, B. Tyson, and R.K. Abu Al-Rub, Carbon Nano Filaments in Cementitious Materials: Some Issues on Dispersion and Interfacial Bond, ACI Symp. Publ. 267 (n.d.). doi:https://doi.org/10.14359/51663280.

[34] C. Gay, F. Sanchez, Performance of carbon nanofiber-cement composites with a high-range water reducer, Journal of the Transportation Research Board 2142 (2010) 109-113. doi:https://doi.org/10.3141/2142-16.

[35] B. Tyson, R.K. Abu Al-Rub, A. Yazdanbakhsh, Z. Grasley, Carbon Nanotubes and Carbon Nanofibers for Enhancing the Mechanical Properties of Nanocomposite Cementitious Materials, J. Mater. Civ. Eng. 23 (2011) 1028–1035. doi:http://doi.org/10.1061/(ASCE)MT.1943-5533.0000266.

[36] X. Wang, I. Rhee, Y. Wang, Y. Xi, Compressive strength, chloride permeability, and freeze-thaw resistance of MWNT concretes under different chemical treatments, The Scientific World Journal (2014) 572102. https://doi.org/10.1155/2014/572102.

[37] S. Sharma, N.C. Kothiyal, Facile growth of carbon nanotubes coated with carbon nanoparticles: A potential low-cost hybrid nanoadditive for improved mechanical, electrical, microstructural and crystalline properties of cement mortar matrix, Constr. Build. Mater. 123 (2016) 829–846. doi:https://doi.org/10.1016/j.conbuildmat.2016.07.045.

[38] L.I. Nasibulina, I.V. Anoshkin, S.D. Shandakov, A.G. Nasibulin, A. Cwirzen, P.R. Mudimela, K. Habermehl-Cwirzen, J.E.M. Malm, T.S. Koltsova, Y. Tian, E.S. Vasilieva, V. Penttala, O.V. Tolochko, M.J. Karppinen, E.I. Kauppinen, Direct synthesis of carbon nanofibers on cement particles, Journal of the Transportation Research Board 2142 (2010) 96-101. doi:https://doi.org/10.3141/2142-14.

[39] S. Sun, X. Yu, B. Han, J. Ou, In situ growth of carbon nanotubes/carbon nanofibers on cement/mineral admixture particles: A review, Constr. Build. Mater. 49 (2013) 835–840. doi:https://doi.org/10.1016/j.conbuildmat.2013.09.011.

[40] P.R. Mudimela, L.I. Nasibulina, A.G. Nasibulin, A. Cwirzen, M. Valkeapaa, K. Habermehl-Cwirzen, J.E.M. Malm, M.J. Karppinen, V. Penttala, T.S. Koltsova, O.V. Tolochko, E.I. Kauppinen, Synthesis of carbon nanotubes and nanofibers on silica and cement matrix materials, Journal of Nanomaterials (2009) 526128. doi:https://doi.org/10.1155/2009/526128

[41] S. Sharma, N.C. Kothiyal, Synergistic effect of zero-dimensional spherical carbon nanoparticles and one-dimensional carbon nanotubes on properties of cement-based ceramic

matrix: microstructural perspectives and crystallization investigations, Composite Interfaces, 22(9) (2015) 899-921. doi:https://doi.org/10.1080/09276440.2015.1076281

[42] M. Jung, Y. Lee, S.-G. Hong, J. Moon, Carbon nanotubes (CNTs) in ultra-high performance concrete (UHPC): Dispersion, mechanical properties, and electromagnetic interference (EMI) shielding effectiveness (SE), Cem. Concr. Res. 131 (2020) 106017. doi:https://doi.org/10.1016/j.cemconres.2020.106017.

[43] W. Meng, K.H. Khayat, Effect of graphite nanoplatelets and carbon nanofibers on rheology, hydration, shrinkage, mechanical properties, and microstructure of UHPC, Cem. Concr. Res. 105 (2018) 64–71. doi:https://doi.org/10.1016/j.cemconres.2018.01.001.

[44] W. Meng, K.H. Khayat, Mechanical properties of ultra-high-performance concrete enhanced with graphite nanoplatelets and carbon nanofibers, Compos. Part B Eng. 107 (2016) 113–122. doi:https://doi.org/10.1016/j.compositesb.2016.09.069.

[45] ASTM C1856 / C1856M-17, Standard Practice for Fabricating and Testing Specimens of Ultra-High Performance Concrete, ASTM International, West Conshohocken, PA, 2017. doi:http://doi.org/10.1520/C1856_C1956M-17.

[46] ASTM C33 / C33M-18, Standard Specification for Concrete Aggregates, ASTM International, West Conshohocken, PA, 2018. doi:http://doi.org/10.1520/C0033_C0033M-18.

[47] E.M. Williams, S.S. Graham, P. Reed, P., and T.S. Rushing, Laboratory Characterization of Cor-Tuf Concrete With and Without Steel Fibers (2009).

[48] B.A. Graybeal, Characterization of the behavior of ultra-high-performance concrete (Doctoral dissertation). (2005).

[49] M. Shafieifar, M. Farzad, A. Azizinamini, Experimental and numerical study on mechanical properties of Ultra High Performance Concrete (UHPC), Constr. Build. Mater. 156 (2017) 402–411. doi:https://doi.org/10.1016/j.conbuildmat.2017.08.170.

[50] ASTM C192 / C192M-19, Standard Practice for Making and Curing Concrete Test Specimens in the Laboratory, ASTM International, West Conshohocken, PA, 2019. doi:http://doi.org/10.1520/C0192_C0192M-19.

[51] M. Bediako, J.T. Kevern, E.O. Amankwah, Effect of Curing Environment on the Strength Properties of Cement and Cement Extenders, Materials Sciences and Applications, 6 (2015) 33-39. doi:https://doi.org/10.4236/msa.2015.61005.

[52] B. Lothenbach, F. Winnefeld, C. Alder, E. Wieland, P. Lunk, Effect of Temperature on the Pore Solution, Microstructure and Hydration Products of Portland Cement Pastes, Cement and Concrete Research, 37 (2007) 483-491. doi:https://doi.org/10.1016/j.cemconres.2006.11.016.

[53] P. Ballester, A. Hidalgo, I. Mármol, J. Morales, L. Sánchez, Effect of Brief Heat-Curing on Microstructure and Mechanical Properties in Fresh Cement Based Mortars, Cement and Concrete Research, 39 (2009) 573-579. doi:https://doi.org/10.1016/j.cemconres.2009.04.002.

[54] ASTM C348-20, Standard Test Method for Flexural Strength of Hydraulic-Cement Mortars, ASTM International, West Conshohocken, PA, 2020. doi:http://doi.org/10.1520/C0348-20.

[55] ASTM C1074-19e1, Standard Practice for Estimating Concrete Strength by the Maturity Method, ASTM International, West Conshohocken, PA, 2019. doi:http://doi.org/10.1520/C1074-19E01.

[56] ASTM C1064 / C1064M-17, Standard Test Method for Temperature of Freshly Mixed Hydraulic-Cement Concrete, ASTM International, West Conshohocken, PA, 2019. doi:http://doi.org/10.1520/C1064_C1064M-17.

[57] ASTM C1585-20, Standard Test Method for Measurement of Rate of Absorption of Water by Hydraulic-Cement Concretes, ASTM International, West Conshohocken, PA, 2020. doi:http://doi.org/10.1520/C1585-20.

[58] ASTM C1543-10a, Standard Test Method for Determining the Penetration of Chloride Ion into Concrete by Ponding (Withdrawn 2019), ASTM International, West Conshohocken, PA, 2010. doi:http://doi.org/10.1520/C1543-10A.

[59] AASHTO T260, Standard Method of Test for Sampling and Testing for Chloride Ion in Concrete and Concrete Raw Materials, Washington, D.C., 1998.

[60] Y. Xi, L. Li, and R. Railsback, Evaluation of different types of waterproofing membranes (asphaltic and non-asphaltic) as cost effective bridge deck barriers in reducing corrosive chloride effects, Colorado Depart. Trans. Appl. Res. Innov. Branch, June, 2018.

[61] ASTM C39 / C39M-21, Standard Test Method for Compressive Strength of Cylindrical Concrete Specimens, ASTM International, West Conshohocken, PA, 2021. doi:http://doi.org/10.1520/C0039_C0039M-21.

[62] ASTM C143 / C143M-20, Standard Test Method for Slump of Hydraulic-Cement Concrete, ASTM International, West Conshohocken, PA, 2020. doi:http://doi.org/10.1520/C0143_C0143M-20.

[63] ASTM C830-00(2016), Standard Test Methods for Apparent Porosity, Liquid Absorption, Apparent Specific Gravity, and Bulk Density of Refractory Shapes by Vacuum Pressure, ASTM International, West Conshohocken, PA, 2016. doi:http://doi.org/10.1520/C0830-00R16.

[64] M. Ramezani, Y.H. Kim, Z. Sun, Modeling the mechanical properties of cementitious materials containing CNTs, Cem. Concr. Compos. 104 (2019) 103347. doi:https://doi.org/10.1016/j.cemconcomp.2019.103347.

[65] F.R. Furtado de Mendonca, M.A. El-Khier, G. Morcous, J. Hu, Feasibility study of development of Ultra-high performance concrete (UHPC) for highway bridge applications in Nebraska, Nebraska Department of Transportation Research Reports, (2020) 242.

[66] AFGC-SETRA (Association Francaise de Genie Civil-Service d'etudes Techniques des Routes et Autoroutes), Ultra-high performance fibre-reinforced concretes, recommendations provisoires-interim recommendations, 2002, pp. 98.

[67] Abbas, S., Nehdi, M.L. & Saleem, M.A. Ultra-High Performance Concrete: Mechanical Performance, Durability, Sustainability and Implementation Challenges. Int. J. Concr. Struct. Mater. 10 (2016), 271–295. https://doi.org/10.1007/s40069-016-0157-4.

[68] M. Malusis, J. Evans, M. McLane, N. Woodward, A Miniature Cone for Measuring the Slump of Soil-Bentonite Cutoff Wall Backfill, Geotech. Test. J. 31 (2008) 373–380. doi:http://doi.org/10.1520/GTJ101487.

[69] S. Clayton, T.G. Grice, D. V Boger, Analysis of the slump test for on-site yield stress measurement of mineral suspensions, Int. J. Miner. Process. 70 (2003) 3–21. doi:https://doi.org/10.1016/S0301-7516(02)00148-5.

[70] ASTM C1202-19, Standard Test Method for Electrical Indication of Concrete's Ability to Resist Chloride Ion Penetration, ASTM International, West Conshohocken, PA, 2019. doi:http://doi.org/10.1520/C1202-19.

[71] T. Wang, J. Xu, B. Meng, G. Peng, Experimental study on the effect of carbon nanofiber content on the durability of concrete, Constr. Build. Mater. 250 (2020) 118891. doi:https://doi.org/10.1016/j.conbuildmat.2020.118891.

[72] M.S. Konsta-Gdoutos, P.A. Danoglidis, S.P. Shah, High modulus concrete: Effects of low carbon nanotube and nanofiber additions, Theor. Appl. Fract. Mech. 103 (2019) 102295. doi:https://doi.org/10.1016/j.tafmec.2019.102295.

[73] E. John, T. Matschei, D. Stephan, Nucleation seeding with calcium silicate hydrate – A review, Cem. Concr. Res. 113 (2018) 74–85. doi:https://doi.org/10.1016/j.cemconres.2018.07.003.

[74] S. Muzenski, I. Flores-Vivian, K. Sobolev, Ultra-high strength cement-based composites designed with aluminum oxide nano-fibers, Constr. Build. Mater. 220 (2019) 177–186. doi:https://doi.org/10.1016/j.conbuildmat.2019.05.175.

Appendix A

Table A1 Materials

Materials	Sources
Type I Portland cement	Cemex Inc.
Silica fume	Grade 971, Elkem
All-purpose natural sand	Quikrete Inc.
Milliken USGA natural sand	BURNCO Inc.
Silica powder	Size #325, AGSCO Co.
HRWR	MasterGlenium 7920, BASF Inc.
CNFs (PR-19-XT-PS)	Pyrograf Products Inc.